AD-A194 253 FLOW DYNAMICS STIMULATED BY HAIRPIN-LIKE VORTICES IN 1/1
INITIALLY LAMINAR BO..(U) SCIENTIFIC RESEARCH
ASSOCIATES INC GLASTONBURY CT N S LIU ET AL. 31 MAR 88
UNCLASSIFIED SRA-R88-910016-A AFOSR-TR-88-0473 F/G 20/4 NL

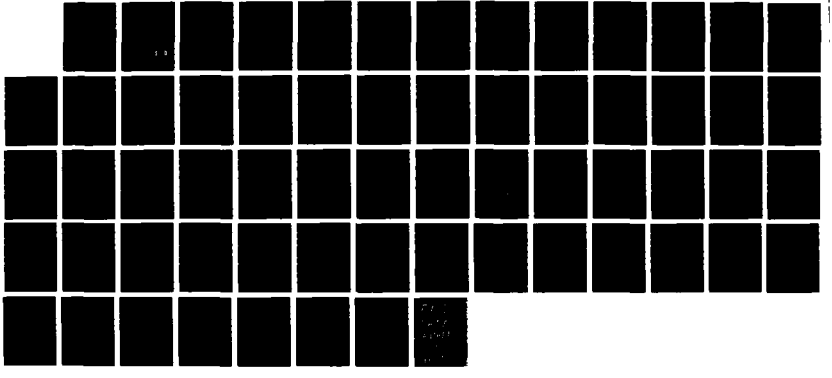

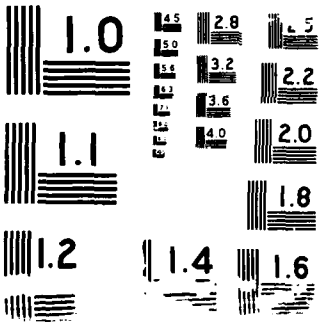
1.0
1.1
1.2
1.4
1.6
1.8
2.0
2.2
2.8
3.2
3.6
4.0
4.5
5.0

(2)

Report R88-910016-A

FLOW DYNAMICS STIMULATED BY HAIRPIN-LIKE VORTICES IN INITIALLY LAMINAR BOUNDARY LAYERS

N.S. Liu, S.J. Shamroth and H. McDonald
Scientific Research Associates, Inc
P.O. Box 1058
Glastonbury, CT 06033

Annual Report, March 1988

Prepared for:
Air Force Office of Scientific Research
under Contract F49620-86-C-0028

UNCLASSIFIED

SECURITY CLASSIFICATION OF THIS PAGE

REPORT DOCUMENTATION PAGE AD-A194253

Form Approved OMB No. 0704-0188

1a. REPORT SECURITY CLASSIFICATION: Unclassified	1b. RESTRICTIVE MARKINGS
2a. SECURITY CLASSIFICATION AUTHORITY	3. DISTRIBUTION/AVAILABILITY OF REPORT: Distribution unlimited
2b. DECLASSIFICATION/DOWNGRADING SCHEDULE	
4. PERFORMING ORGANIZATION REPORT NUMBER(S): R88-910016-A	5. MONITORING ORGANIZATION REPORT NUMBER(S): AFOSR-TR- 88-0473
6a. NAME OF PERFORMING ORGANIZATION: Scientific Research Associates; 6b. OFFICE SYMBOL (If applicable): 8N189	7a. NAME OF MONITORING ORGANIZATION: AFOSR
6c. ADDRESS (City, State, and ZIP Code): 50 Nye Road, P.O. Box 1058, Glastonbury, CT 06033	7b. ADDRESS (City, State, and ZIP Code): AFOSR/NA, Bolling AFB, DC 20332
8a. NAME OF FUNDING/SPONSORING ORGANIZATION: Air Force Office of Scientific Research; 8b. OFFICE SYMBOL (If applicable): NA	9. PROCUREMENT INSTRUMENT IDENTIFICATION NUMBER: F49620-86-C-0028
8c. ADDRESS (City, State, and ZIP Code): Building 410, Bolling Air Force Base, D.C. 20332-6448	10. SOURCE OF FUNDING NUMBERS: PROGRAM ELEMENT NO. 61102F; PROJECT NO. 3005; TASK NO A1; WORK UNIT ACCESSION NO.

11. TITLE (Include Security Classification)

FLOW DYNAMICS STIMULATED BY HAIRPIN-LIKE VORTICES IN INITIALLY LAMINAR BOUNDARY LAYERS

12. PERSONAL AUTHOR(S): N.S. Liu, S.J. Shamroth and H. McDonald

13a. TYPE OF REPORT	13b. TIME COVERED	14. DATE OF REPORT (Year, Month, Day)	15. PAGE COUNT
Annual	FROM 87FEB01 TO 88JAN31	88March31	57

16. SUPPLEMENTARY NOTATION

17. COSATI CODES		
FIELD	GROUP	SUB-GROUP

18. SUBJECT TERMS (Continue on reverse if necessary and identify by block number)

Organized Flow Events, Hairpin Vortices, Direct Numerical Simulation,

19. ABSTRACT (Continue on reverse if necessary and identify by block number)

Time-marching spatial simulations of flow events stimulated by hairpin-like vortices in the near-wall region of initially laminar boundary layers are in progress. The behavior characteristics and the underlying physical mechanisms are being examined by using three distinct but related methods of analysis. The results presented in this ~~Annual~~ Report are the kinematic and dynamic states in a plane at a given instant. The spatial distributions of various flow quantities over a cross-section of the streamwise vortex have been examined and interpreted. These quantities are: translational velocity, vorticity, production of vorticity due to straining, viscous diffusion of vorticity, dissipation, static pressure and viscous stress tensor. Such a local, instantaneous analysis forms the basis for a global temporal analysis; its results will be presented in the Final Report. Keywords:

20. DISTRIBUTION/AVAILABILITY OF ABSTRACT	21. ABSTRACT SECURITY CLASSIFICATION	
☒ UNCLASSIFIED/UNLIMITED ☐ SAME AS RPT. ☐ DTIC USERS	Unclassified	
22a. NAME OF RESPONSIBLE INDIVIDUAL: Dr. James McMichael	22b. TELEPHONE (Include Area Code): (202) 767-4936	22c. OFFICE SYMBOL: NA

DD Form 1473, JUN 86 — Previous editions are obsolete. — SECURITY CLASSIFICATION OF THIS PAGE

UNCLASSIFIED

ABSTRACT

Time marching spatial simulations of flow events stimulated by hairpin vortices in the near-wall region of initially laminar boundary layers are in progress. The behavioral characteristics and the underlying physical mechanisms are being examined by using three distinct but related methods of analysis. The results presented in this Annual Report are the kinematic and dynamic states in a plane at a given instant. The spatial distributions of various flow quantities over a cross-section of the streamwise vortex have been examined and interpreted. These quantities are: translational velocity, vorticity, production of vorticity due to straining, viscous diffusion of vorticity, dissipation, static pressure and viscous stress tensor. Such a local, instantaneous analysis forms the basis for a global temporal analysis; its results will be presented in the Final Report.

TABLE OF CONTENTS

I. INTRODUCTION

The occurrence of large-scale identifiable structures in turbulent flows has been well-known for quite some time. However, these organized aspects of turbulence were not recognized as characteristic features of transitional as well as fully-developed turbulent flows until the last decade. It is the recognition of the widespread occurrence of organized structures and their dominant dynamical role in turbulence production and transport which has been one of the driving factors in recent turbulence research. The organized (or coherent)-structure approach to turbulence presents the potential for better understanding turbulence phenomena and perhaps developing a structure-incorporated theory of turbulence. The understanding of organized structures clearly holds the key to understanding the management and control of turbulence. There are already evidences of technological benefits derived from the turbulence management via coherent structure manipulations using passive and active controls. Thus, the organized-structure approach to the turbulence research should not be viewed as merely of conceptual interest; this approach is of profound practical significance [1].

The studies of organized structures in turbulent flows have been pursued in two different forms: laboratory experiments and computer experiments (i.e. numerical simulations). Each form has its own technological and economic advantages and constraints. Consequently, they represent complementary approaches for progressing in this problem area. Since the complementary use of laboratory and computer experiments provides the most promising approach to increasing our capability in the coherent structure field, it is appropriate to fully review some aspects of both areas, even though the present effort is a purely computational one. In the context of laboratory experiments, the overwhelming majority of the investigations of organized structures to date have been based on flow visualization. Flow visualization represents a very useful tool in coherent structure investigations. These studies have led to significant progress in understanding flow mechanisms. However, flow visualization does contain limitations which must be recognized in assessing the results. First of all, much of the flow visualization work has been performed at low Reynolds number. Secondly, the results must be interpreted, recognizing the possible high Schmidt number of markers and the inevitable history integration effects. These drawbacks result in flow visualization

being regarded as a very useful, nevertheless qualitative, tool. The second experimental approach is based upon hot wire or LDA measurements. As constrained by current measurement technology, time records of flow variables at fixed spatial points are provided by relatively few sensors. A spatial description is then deduced from temporal information obtained from these stationary sensors. The use of data obtained from stationary sensors to develop an understanding of the flow mechanisms associated with a coherent structure moving past the sensor obviously contains its own set of assumptions; e.g. Taylor's hypothesis. Considering both the flow visualization approach and the stationary sensor approach, it is clear that both flow visualization and simultaneous signal analysis should be applied in organized structure investigations and attempts should be made to combine the results obtained from these two approaches into a single consistent picture [2]. These blended results would greatly aid the establishment of a generic and robust technique for the eduction of coherent structures or events in turbulent flows. The success of the coherent-structure approach to the turbulence depends on such an eduction scheme.

Many computer experiments have focused upon developing understanding of the role of vortical structures in the cyclic turbulence process. The most common approach is a Lagrangian approach based on numerical approximations of the Biot-Savart integral, which tracks the evolving trajectory and shape of vortical structures forward in time [3]. Since the Biot-Savart integral is purely kinematic, the success of this approach in simulating the flow physics greatly depends on the ability of prescribing a vortex model with assumed parameters (e.g. the instantaneous local core size and shape) which is dynamically consistent during the entire time span of evolution. This is not an easy task and, consequently, many of these results need to be reassessed in regard to their being a dynamically consistent model. For understanding the causes and effects of the cyclic bursting process observed in turbulent boundary layers, some progress has been made with simpler two-dimensional flows in establishing the effects of convected vortex motions on viscous flows near a wall [4]. In this connection, there is a clear need to develop rational methods for the accurate calculation of flows with multiple three-dimensional vortical structures, the interaction of these structures with each other and solid boundaries, and the behavior of such structures in wall-shear flows.

With the advent of supercomputers, direct numerical simulations of transitional [5],[6] and fully-developed turbulent flows [7] via the solution of time-dependent, three-dimensional, incompressible Navier-Stokes equations are now possible at low and moderate Reynolds numbers. The overwhelming majority of these direct numerical simulations are carried out for plane channel flow using spectral methods. Although plane channel flow has some similarity to boundary layer flow, the laminar channel flow has significantly different stability characteristics than does a laminar boundary layer. Furthermore, in the fully-developed laminar channel flow, the Reynolds number is constant in the flow direction, while the Reynolds number in a laminar boundary layer increases continually in the flow direction. The turbulent boundary layer flow and turbulent channel flow have significantly different characteristics in the outer region, but are very similar in the near-wall region. It should also be noted that the laboratory experiments and numerical experiments using spectral methods do not necessarily address the same problem. For example, the former is evolving in space; the latter is evolving in time, as it uses periodic boundary conditions in flow direction. In spite of these differences, the agreement between experiments and these simulations is very encouraging. Nevertheless, some problem areas are evident.

Current numerical simulations are limited both in resolution (hence flow Reynolds number) and in the duration of flow time that can be economically computed. The Reynolds number of flows that can be computed directly is rather small when compared with practical or even laboratory turbulent flows. Adequate computation time for the eduction of coherent structures or for obtaining phase-average analysis of flow variables is extremely, if not prohibitively, expensive. In addition, the analysis of the data generated by simulation in itself is quite challenging. The amount of numerical data which is obtained from a direct numerical simulation represents a very extensive and complex data base which contains all of the data reduction problems present in the results of a detailed experiment. The vast amount of data present may obscure a detailed understanding of the basic turbulence phenomena and, in particular, may obscure the dynamic role of these structures in turbulence production and transport. The focus of the effort being performed under the present contract effort is to highlight this dynamic role.

II. MOTIVATION AND BASIS OF THE PRESENT EFFORT

In turbulent boundary layer flows, it is now widely accepted that near-wall organized (or coherent) structures play a major role in production and control of turbulence. Three types of structures have been identified experimentally. These are: (1) hairpin vortices, (2) elongated, streamwise counter-rotating vortices near the wall, and (3) ring vortices. One particular laboratory study giving very convincing evidence for the existence of hairpin vortices in fully-developed turbulent boundary layers is provided by Head and Bandyophadyay [8]. From an extensive series of experiments using both smoke flow-visualization and hot-wire measurements, they concluded that turbulent boundary layers up to $Re_\theta \approx 10^4$ consist substantially of hairpin-shaped vortex loops arrayed at a characteristic angle of approximately 45° to the wall toward the downstream direction. The spanwise spacing of these structures appears to follow the Kline scaling of approximately 100. Perry and Chong [9] demonstrated that the existence of a hierarchy of hairpin vortices is consistent with a logarithmic time-mean velocity profile. The mean velocity distribution, broad-band turbulence intensity distributions, and the turbulence spectra can be derived from this assumed hierarchy of hairpin vortex structures. Based upon an examination of several direct and large-eddy simulation calculations of turbulent channel flow, Moin and Kim [10] indicated that the hairpin vortices are the characteristic structures of all wall-bounded flows, irrespective of their outer boundary conditions. The preponderant appearance and dominant dynamical role of hairpin vortices in turbulent boundary layers naturally leads to the following questions: How can we better understand them? How can we use these structures to advantage?

In a turbulent environment, there is jitter both in the initiation of successive structures and in the structure trajectory or evolution. It is also known that the evolution of a large-scale turbulence structure can depend on the conditions of any other structures which are simultaneously present, as well as the background incoherent turbulence. Thus, the sensitivity of the instantaneous flow to a multitude of flow conditions greatly complicates the identification and analysis of various dynamical processes. Nevertheless, Acarlar and Smith [11] demonstrated that many of the organized structures and events observed in the near-wall region of turbulent boundary layers (e.g., elongated streamwise streaks, bursts, etc.) can be synthetically generated by

the stimulation of hairpin vortices in initially laminar boundary layers. The flow patterns thus created have been documented using flow visualization and hot-film anemometry techniques, and cross-compared with the patterns observed in the near-wall region of a fully-developed turbulent boundary layer. The comparison indicates essential identity between the flow patterns generated by the synthetically created hairpin vortices in a developing laminar boundary layer and many of the predominant flow patterns observed in the near-wall region of a turbulent boundary layer. In addition, velocity measurements were made at various streamwise locations. Results indicate that, with the increase of the distance downstream of the incipient hairpin vortex generation region, the velocity profile eventually develops a remarkable similarity to a turbulent boundary layer velocity profile. A numerical simulation of the flow events and secondary vortical structures stimulated by the presence of a synthetically generated, primary hairpin-like vortex in an initially laminar boundary layer has been independently carried out by Liu, Shamroth and McDonald [12].

Hairpin vortices, being the tractable part of wall turbulence, may contain most of the essential physics of the turbulent boundary layers. Thus, the present effort is motivated by the need to gain more physical understanding of the hairpin vortices. This understanding should cover the topographical descriptions of these vortices, as well as their dynamical significance, including the distributions of flow properties over the spatial extent of the vortices. Entrainment, mixing, heat transfer, drag and aerodynamic noise generation are fields in which better understanding of hairpin vortices should produce substantial technological benefits via manipulation and control of these organized structures.

The present effort focuses upon detailed study of flow dynamics stimulated by the presence of synthetically generated hairpin vortices in initially laminar boundary layers. As indicated by the experimental results reported in Ref. [11], this is a viable approach towards obtaining better understanding of the dynamical role of hairpin vortices in wall turbulence. The feasibility of carrying out numerical simulations for such flow conditions has been demonstrated in Ref. [12]. The observations and conclusions obtained from Refs. [11] and [12] provide the basis of the current organized-structure approach to wall turbulence research.

III. TECHNICAL OBJECTIVES

Since near-wall hairpin vortices play a major role in turbulence production and transport occurring in transitional and fully-developed turbulent boundary layers, the understanding of these vortical structures holds the key to the management and control of wall turbulence. The identification and analysis of primary dynamical processes stimulated by a hairpin vortex in fully turbulent environments are greatly complicated by the presence of jitters, incoherent turbulence and the appearance of many other similar structures. Therefore, an approach is required which can elucidate the basic dynamic processes associated with the hairpin vortex. One particular viable approach for gaining an increased physical understanding of these organized structures is to study the flow dynamics stimulated by synthetically generated hairpin vortices in developing laminar boundary layers. The goal of the present effort is to perform such studies using time-marching spatial simulation via direct solution of compressible Navier-Stokes equations, followed by data analysis focusing upon the dynamical significance of hairpin vortices to entrainment, mixing and turbulence production. More specifically, the major objectives of the present work are:

(1) To complete time-marching spatial simulations of flow events stimulated by synthetically generated hairpin-like vortices in initially laminar boundary layers.

(2) To provide evaluated results obtained from the numerical simulations which are further analyzed with Eulerian, Lagrangian and Topological methods of analysis.

(3) To extract and explain the underlying physical processes of the cyclic entrainment, mixing and production of wall turbulence.

(4) To provide a protocol for:
   - Developing a consistent interpretation from flow visualizations and flow measurements;
   - Assessing possible turbulence management and control via the manipulation of hairpin vortices;
   - Assessing possible development of turbulence theory or models explicitly incorporating the dynamics of organized structures.

IV. METHODOLOGY-NUMERICAL SIMULATION

IV.1 Data Acquisition

The unsteady, three-dimensional, compressible Navier-Stokes equations, supplemented by an equation of state and together with the constant total temperature assumption, form the system governing the flows in the present effort. The total temperature assumption was made solely to conserve computer run time and can be easily removed through inclusion of an energy equation. Solutions of the governing equations with moderate Reynolds number and low freestream Mach number, subjected to prescribed initial condition and appropriate boundary conditions, are sought by a numerical procedure termed the consistently split linearized block implicit (LBI) scheme [13]. This technique leads to systems of coupled linear difference equations having narrow block-banded matrix structures which can be solved efficiently by standard block-elimination methods.

As indicated in Section I, the overwhelming majority of direct numerical simulations have been carried out for fully developed plane channel flow using spectral methods. Although fully-developed plane channel flow is quite similar to boundary layer flow, significant differences between these two types of flow do exist, particularly in the outer flow region. Furthermore, many simulations using spectral methods are essentially temporal simulations. Consequently, the results must be transformed to some equivalent spatial simulation by employing a viable transformation. The present numerical approach allows the specification of inflow-outflow as well as freestream conditions. Thus, the present simulations are spatial simulations describing the time-evolution of spatial structures in a physical flow domain containing a boundary layer. In this respect, the present numerical simulation is closer to laboratory experiments. It is quite clear that the present numerical simulation technique also allows the study of effects of compressibility and pressure gradient on the organized structures in boundary layers.

IV.2 Data Analysis

The present analysis of the data generated by numerical simulations focuses upon detailed understanding of the dynamic roles of hairpin vortices in

bursting, entrainment and mixing activities. These are primary sources of turbulence production and transport in turbulent boundary layers. In order to identify the presence of any organized structure and assess its dynamical significance, the present data analysis views an organized structure as being a connected fluid mass with large-scale and instantaneously coherent vorticity over its spatial extent. The identification with fluid mass does not imply that structure evolution is by advection alone, as structure changes by entrainment and interaction with other structures which are simultaneously present in the flow. Since organized structures are associated with fluid mass which are spatially non-overlapping (each has its own territory), it would be inappropriate to view them as waves. Further, a cascade is not a relevant concept for organized structure interactions. Unlike a cascade, when 'eddies' of different scales superimposed upon the same space are presumed to exist in equilibrium, interactions of organized structures always generate newer structures of different scales. It is also noted here that organized structures are not necessarily long-lived, as they interact with other structures, and their survival distance typically decreases with increasing Reynolds number.

Thus, the present data analysis uses coherent vorticity as the primary identifier of organized structures, which have distinct boundaries and independent territories. Naturally, the flow dynamics stimulated by the presence of these structures is to be studied via the vorticity dynamics, supplemented by an investigation of the role of static pressure. Particular attention will be paid to the vortex straining (i.e., stretching and tilting); it has been suggested that vortex straining is the physical mechanism for entrainment, production and continual replenishment of structure turbulence in all turbulent flows.

The present data analysis consists of (1) identification of evolving hairpin vortices and organized structures stimulated by their presence, (2) description of the distributions of various flow properties over the spatial extent of the vortices or structures, and (3) explanation for entrainment, mixing and turbulence production from the view point of vorticity dynamics. In order to achieve these goals, three distinct but related approaches will be employed: (a) Eulerian analysis, which describes flow properties at points fixed in three-dimensional space, this is the data form directly provided by the solution of the Navier-Stokes equations; (b) Lagrangian analysis, which

describes flow properties associated with fixed fluid particles advecting in the three-dimensional flow domain; and (c) Topological analysis, which describes flow properties associated with critical regions or points as viewed from some reference coordinates moving with specified celerity. The Lagrangian and Topological analyses require further processing of data supplied by the solution of Navier-Stokes equations. Subsequently, the results obtained from these three types of analysis will be blended over the flow domain to elucidate the behavioral characteristics of the flow and to extract the underlying physical mechanisms.

Under certain circumstances, it is beneficial to study the data via decomposition of the instantaneous values. The primary data decomposition technique used in the present effort is to split any instantaneous value into two parts: the first component is the initial steady laminar value without the presence of any structure; the second component represents the unsteady variation due to the presence of organized structures. If it is deemed appropriate, decomposition of instantaneous data in terms of some ensemble-averaged value will also be performed to provide some statistical information. Another aspect of the analysis of time-dependent three-dimensional flow data is the effective and efficient display of this information; both two-dimensional plots in appropriate planes and three-dimensional perspective plots are to be used to analyze and evaluate the results of simulation.

V. ANALYSIS

V.1 The Incipient Hairpin Vortex

Although the present study determines the dynamic behavior of a hairpin vortex immersed in a shear flow via a solution of the time-dependent, three-dimensional Navier-Stokes equations, it is necessary to specify an initial flow field; i.e., a flow field at $t = 0$, which includes an incipient vortex structure. This field is based upon a hairpin vortex model. A hairpin vortex is considered here as a slender tube-like region in which the bulk of vorticity is concentrated. Over each cross-section of this tube-like region, a mean direction, $\vec{e}_s$, as well as the strength, Γ, of the concentrated vorticity can be determined. Further, inside of this compact region, a spatial curve can be found such that its tangent is parallel to $\vec{e}_s$ at each cross-section, this

spatial curve is considered as the effective centerline of the slender yet highly vortical region, the position vector of this effective centerline is denoted by $\vec{r}_c$ and a segment of this line is denoted by $d\vec{s} = ds\vec{e}_s$.

When viewed from a region sufficiently away from the effective centerline, the slender hairpin vortex is reduced to a curved line vortex of strength Γ and with position vector $\vec{r}_c$. The signature of the hairpin vortex in this outer region is then the induced velocity field given by the Biot-Savart law:

$$\vec{v}(\vec{r}) = -\frac{1}{4\pi}\int_c \frac{\Gamma(\vec{r}_c-\vec{r})}{\left|\vec{r}_c-\vec{r}\right|^3}\times d\vec{s} \qquad (1)$$

where $\vec{r}$ is the position vector of a point P in the space and $\vec{r}_c$ is the position vector of a point along the line vortex C.

However, when a point P is located in the proximity of the hairpin vortex, the effects of the inner structure of the vortex on the induced field must be taken into account. Although this can be accomplished by using a so-called optimum similarity solution to prescribe the diffusive core structure, the present work employs a simpler model to account for the influence of the diffusive vortex core by multiplying the induced velocity obtained in Eq. (1) with a factor

$$f(d,r_0) = \frac{d^2}{d^2+r_0^2} \qquad (2)$$

where $d = \left|\vec{r}-\vec{r}_c\right|$ and r_0 is the effective core radius. Note that if the solid-body-rotation model were used for simulating the core structure, the multiplying factor would be the minimum between 1 and d^2/r_0^2.

There is considerable evidence that the hairpin vortices originate from the region very close to the wall, in addition, it has been proposed that the configuration of the hairpin vortices in the wall region consists of trailing vortex pairs running along the wall. These trailing vortex pairs often have been referred as counter-rotating vortex pairs of elongated streamwise extent in the wall region of the flow. Aside from the appearance of these trailing vortex pairs in the immediate neighborhood of the wall, the

hairpin vortex as a whole must induce an internal shear layer within the pre-existing boundary layer such that the induced velocity field also satisfies the non-slip condition along the wall. Very little is known about the structure of this induced, unsteady internal shear layer. The present model of the incipient hairpin vortex neglects the details of the trailing vortex pairs and the induced internal shear layer in the region very close to the wall. It is assumed that the effects of their presence are to maintain the attachment of the hairpin vortex to the wall, and to provide a rapid change of the induced velocity field in the region very close to the wall such that the no-slip condition is satisfied. These effects are accounted for by including the wall images of the hairpin vortices when their associated induced velocity fields are evaluated and, in addition, by multiplying the induced velocity fields with a factor

$$g(y) = \ell(y)/\ell_0 \tag{3}$$

where y is the distance from the wall and

$$\ell(y)/\ell_0 = \tanh(\kappa y/\ell_0)\ D \tag{4}$$

with

$$D = 1 - \exp(-y/\ell_1) \tag{5}$$

and κ is the von Karman constant; ℓ_0 and ℓ_1 are some characteristic length scales.

Such a model of induced internal shear layer is based upon Prandtl's mixing length theory which assumes that the velocity fluctuations in the near wall region are proportional to some length scale $\ell(y)$. The present work further assumes that the distribution of $\ell(y)$ is given by Eqs. (4) and (5), which are similar in their forms to the conventional mixing length model, except that ℓ_0 is considered here as a vertical length scale representing the conjectured thickness of the induced internal shear layer and ℓ_1 is considered here as a vertical length scale on which the near wall damping becomes important. Typically, ℓ_0 can be chosen as a small fraction of the height of the hairpin vortex and ℓ_1 is approximately equal to ℓ_0. It is stressed here that this model of induced internal shear layer is used only for constructing the initial

induced flow field associated with the imposed hairpin vortex, and it is not used in the subsequent calculations.

As mentioned before, the hairpin vortex has a general shape resembling a rounded-top horseshoe. The Biot-Savart integral, i.e. Eq. (1), for a curved vortex filament formally contains singular terms. Although these singular terms can be removed by analytical cancellation, in addition to the prescription of models of diffusive core structure such as the one given by Eq. (2), considerable mathematical and computational complexities are involved with the evaluation of the induced velocity field of a curved vortex filament. The present work assumes that the precise shape of the incipient hairpin vortex is not of major importance; therefore, for simplicity in setting the initial flow field for the Navier-Stokes simulation, the legs of the hairpin vortex will be assumed to be straight and merge at a sharp point. As for the orientation of the incipient hairpin vortex, the inclination angle between the vortex and the wall is mainly determined by the balance between the self-induced strain field and the strain field provided by the background flow. For a hairpin vortex extending from the wall to the outer edge of the boudary layer, the inclination angle is not uniformly 45°. In the close vicinity of the wall, the inclination of the trailing vortex pairs is much smaller than the 45° angle, while near the outer edge of the boundary layer it is much larger than the 45° angle, nevertheless, over a substantial portion of the hairpin vortex, the legs remain essentially straight with a characteristic inclination angle of 45°. After setting this initial flow, the hairpin vortex development is governed by the solution of the three-dimensional, time-dependent Navier-Stokes equations. In addition, it is assumed that the hairpin vortices appear mostly in the form of an array in the spanwise direction, and members of the same array of vortices have identical properties. Such an assumption implies that the hairpin vortices are produced by the evolution of an initially spanwise-oriented two-dimensional vortex line into a three-dimensional wavy structure which is periodic in the spanwise direction.

Based on the above discussions, the model of the incipient hairpin vortex used in the present work consists of a spanwise array of identical vortices. The effective centerline of these vortices forms an array of interconnecting isosceles triangles which are periodic in the spanwise direction. In setting the initial flow field, the strength of these vortices does not vary along the effective centerline which inclines to the wall at an angle of 45°. In order

to maintain the attachment of these vortices to the rigid wall, their wall images are also included. The effects of the inner core structure of these vortices are accounted for by introducing a diffusive factor into the evaluation of the associated induced velocity field. In addition, the existence of an induced internal shear layer in the immediate neighborhood of the wall is accounted for by employing a distributive factor into the evaluation of the induced velocity field.

A schematic of the present model is shown in Fig. 1, where h_i is the height of the i-th array of hairpin vortices, λ_i the spanwise distance between the feet of the vortices, $\phi_i = \phi = 45°$ the characteristic angle and r_{oi} the radius of the effective core. The signature or the induced velocity field of the i-th array of hairpin vortices at a point P with position vector $\vec{r}$ is then given by

$$\vec{v}_i(\vec{r}) = f_i(d_i, r_{oi}) \left[-\frac{\Gamma_i}{4\pi} \int_{c_i} \frac{(\vec{r}_{c_i} - \vec{r})}{|\vec{r}_{c_i} - \vec{r}|^3} \times d\vec{s}_i \right] g_i(y) \qquad (6)$$

with

$$f_i(d_i, r_{oi}) = \frac{d_i^2}{d_i^2 + r_{oi}^2} \qquad (7)$$

and

$$g_i(y) = \tanh(\kappa y/\ell_{oi})[1-\exp(-y/\ell_{li})] \qquad (8)$$

where C_i is the effective centerline of the vortices together with their wall images, and $d_i = |\vec{r}_{ci} - \vec{r}|$. The corresponding vorticity distribution is obtained from

$$\vec{\Omega}_i = \nabla \times \vec{v}_i \qquad (9)$$

Obviously, when the array contains a sufficiently large number of vortices, the induced velocity field $\vec{v}_i$ and hence $\vec{\Omega}_i$ are periodic functions with spatial period λ_i. Therefore, the induced field due to such an array of vortices is

completely defined by the flow field within the spanwise domain of any one member of the vortices. Henceforth, the term 'representative' hairpin vortex will be used to indicate some particular member of the vortex array such that the point P happens to locate within the spanwise domain of this particular vortex (see Fig. 1). It should be noted that the induced flow field within a representative hairpin vortex contains not only the contribution of this vortex but also contains the contributions of all the other vortices in the same array.

Experiences indicate that, by placing approximately 30 or more vortices on each side of the representative vortex, an excellent approximation to the spanwise periodicity required by an infinite number of spanwise vortices can be achieved. In addition, the induced streamwise velocity component $\tilde{u}_i$, the induced normal velocity component $\tilde{v}_i$ and the induced pressure $\tilde{p}_i$ are symmetric about the center plane $\tilde{z} = 0$ (see Fig. 1) while the induced spanwise velocity component $\tilde{w}_i$ is antisymmetric about $\tilde{z} = 0$, where $(\tilde{x},\tilde{y},\tilde{z})$ is a coordinate system attached to some nominal center of the representative vortex at $t = 0$. It also can be shown that the induced field falls off rapidly in regions relatively away from the representative vortex. The vertical extent of the domain of significant influence of the representative vortex is approximately equal to h_i, its streamwise extent is of the order of $\ell_i = h_i \cot \phi_i$, while its spanwise extent remains to be of the order of λ_i.

V.2 Initial and Boundary Conditions

At any instant, the composite flow can be considered as consisting of the background flow and the variation from the background flow. Obviously, such a variation contains not only the evolution of the incipient hairpin vortices, but also the subsequent distortion of the background flow due to these vortices. Let (u,v,w,p) denote the Cartesian velocity components and the pressure of the composite flow observed in a ground-fixed system (x,y,z), where x is in the streamwise direction, y is the distance normal to the wall and z is in the spanwise direction, then

$$u(x,y,z,t) = u'(x,y,z,t) + U(x,y,z) \tag{10}$$

$$v(x,y,z,t) = v'(x,y,z,t) + V(x,y,z) \tag{11}$$

$$w(x,y,z,t) = w'(x,y,z,t) + W(x,y,z) \tag{12}$$

$$p(x,y,z,t) = p'(x,y,z,t) + P(x,y,z) \tag{13}$$

where U, V, W and P are the velocity components and the pressure of the background flow which is considered as nominally steady. The variations from the background flow are denoted by (u',v',w',p').

Solutions of the governing equations with moderate Reynolds number and low freestream Mach number subjected to prescribed initial condition, and appropriate boundary conditions are sought by numerical solution procedure. Generally speaking, the initial conditions as well as the boundary conditions depend on the initial arrangement of the synthetically generated hairpin vortices. The current effort focuses upon the dynamical effects of one 'representative' hairpin vortex submerged in a two-dimensional background flow of boundary layer type. In the following, the initial condition and the boundary conditions for this case are discussed.

The background flow is supplied by performing the usual Navier-Stokes calculation for obtaining boundary layer type of flow with or without significant pressure gradient. The initial velocity field associated with the representative hairpin vortex is constructed with the aid of Biot-Savart law, supplemented by modifications accounting for the effects of diffusive vortical core and the effects of induced internal shear layer, as described by Eq. (6). Since the induced velocity is obtained with Biot-Savart integral, this field is evaluated with respect to a coordinate system $(\tilde{x},\tilde{y},\tilde{z})$ which is attached to some nominal center of the hairpin vortex. It is assumed here that, at t = 0, a representative hairpin vortex is synthetically generated in some region of the background flow such that

$$u'(x,y,z,t=0) = \tilde{u}(\tilde{x},\tilde{y},\tilde{z}) \tag{14}$$

$$v'(x,y,z,t=0) = \tilde{v}(\tilde{x},\tilde{y},\tilde{z}) \tag{15}$$

$$w'(x,y,z,t=0) = \tilde{w}(\tilde{x},\tilde{y},\tilde{z}) \tag{16}$$

with

$$x = \tilde{x} + x_o \tag{17}$$

$$y = \tilde{y} \tag{18}$$

$$z = \tilde{z} \tag{19}$$

i.e. the nominal center is located at the midpoint between the two feet of the hairpin vortex, and it has a streamwise position $x = x_o$. As mentioned before, $\tilde{u}$, $\tilde{v}$ and $\tilde{w}$ are obtained from Eq. (6).

Thus, the initial conditions for u, v and w are completely prescribed. The initial condition for the composite pressure field p must be specified in such a way that it is consistent with the prescribed composite velocity field. By noting that (i) the induced field falls off rapidly in regions away from the hairpin vortex, and (ii) over a very short time span $\Delta t \to 0$; it is quite valid to consider the induced field as frozen, then, the starting pressure field of the composite flow is obtained by using the prescribed velocity field and by integrating the normal momentum equation in its steady form subjected to the following boundary condition

$$p(x,y \to \infty,z,t = 0) = P(x,y \to \infty,z) \tag{20}$$

i.e. $p' \to o$ as $y \to \infty$.

A consistent, initial density field of the composite flow also must be supplied. In general,, this can be accomplished by several iterations between the results of the integration of the normal momentum equation and the solutions of the equation of state. For nearly incompressible flow cases, such an iteration procedure usually can be by-passed.

As for the boundary conditions, non-slip condition is applied on the wall plane and the density on this plane is calculated from the normal momentum equation. On a plane which is parallel to the rigid wall, and is located sufficiently away from the outer edge of the boundary layer, the pressure distribution is specified and the second derivative of the normal velocity

component is considered as zero. In addition, the first derivatives of the streamwise as well as the spanwise velocity components are set to be zero. The streamwise boundary conditions used in the present simulation specify upstream total pressure and downstream static pressure distributions. The upstream total pressure together with specified boundary layer thicknesses and dimensionless boundary layer profiles determine the actual values of the streamwise velocity component at the inflow section. Further, the first derivatives of all the other velocity components and the static pressure are set to be zero. At the downstream boundary, the pressure distribution is specified and the second derivative of streamwise velocity component is set to be zero, while zero first derivatives of all the other velocity components are imposed on the outflow plane. It is noted here that the downstream pressure is specified in an unsteady and nonuniform manner. The unsteadiness and spatial variation of the pressure in the outflow plane are estimated from the flow transients occuring in its neighborhood. The specified values take into account these estimations. These boundary conditions are expected to be appropriate so long as the inflow, outflow and the outer freestream planes are sufficiently far away from the evolving hairpin vortex throughout the course of the simulation. Due to the initial arrangement of the incipient hairpin vortex and the use of a two-dimensional background flow, symmetrical conditions can be applied on the planes $z = -0.5\ \lambda$ and $z = 0$ (see Fig. 1), this completes the specification of boundary conditions in the spanwise direction.

VI. OUTLINES OF THE SIMULATION

The background flow is a zero-pressure-gradient laminar boundary layer flow with a freestream Mach number of 0.4, i.e., it is essentially a Blasius flow. The inflow section of the computational domain is located at a plane where $Re_\delta^* = 419$ and the outflow section is located at a plane where $Re_\delta^* = 576$, where Re_δ^* is the Reynolds number based on freestream velocity and the local displacement thickness. Thus, the computational domain contains both sub-critical and super-critical growth regions, as defined by linear stability theory.

Then, a slanted 'representative' hairpin-like vortex is synthetically generated in the near wall region of the background flow. The inclination angle is 45° toward the downstream direction, the legs of the vortex are

attached to the wall at a place where $Re_{\delta^*} = 487$. The height of this incipient vortex is $h = 0.5\delta_0$ and the spanwise spacing between the vortex feet is $\lambda = 2\delta_0$, where δ_0 is the boundary layer thickness at a place where $Re_{\delta^*} = 490$. The strength of this incipient vortex is so chosen that the maximum magnitude of the induced velocity is 8.5 percent of the freestream velocity.

The flow dynamics stimulated by this incipient hairpin-like vortex in a developing boundary layer is studied by the direct solution of time-dependent, three-dimensional, compressible Navier-Stokes equations. The streamwise extent of the computational domain has a length of $33\delta_0$ covered with 250 grid points, the vertical extent has a length of $5\delta_0$ covered by 55 grid points, and the spanwise extent has a length of δ_0 covered with 15 grid points. The grid spacings are essentially uniform, except for regions close to the boundaries of the computational domain, where appropriate grid stretchings are used. In regard to the size of the time-step used in the unsteady calculation, the CFL numbers based on freestream velocity are uniformly smaller than one. With such a grid distribution and size of the time-step; the spatial and temporal resolutions of the present simulation are expected to be adequate for a time interval during which a freestream particle will travel from the vortex incipient region to the neighborhood of the downstream boundary of the computational domain.

VII RESULTS

The present numerical simulation generates a database containing information about the evolution of an incipient hairpin-like vortex and the events/secondary structures stimulated by its presence in a developing boundary layer. This database needs to be interpreted by applying Eulerian, Lagrangian and Topological data analysis techniques to these unsteady results over a sufficiently long period of flow evolution. At the present time, both the computation and data interpretation are still in progress. A comprehensive description and analysis of the flow dynamics inferred from the simulation will be presented in the Final Report. In the following, some results will be given to indicate certain aspects of the flow development observed during the early stages of the simulation.

The streamwise velocity profiles of the background flow at several streamwise locations are shown in Fig. 2. These profiles are plotted in terms

of the similarity variable $\eta = y/(2\nu x/u_\infty)^{1/2}$. The symbol '*' corresponds to data points provided by the numerical solution, while the theoretical Blasius solution is given by a solid curve. As it can be seen, the background flow is the Blasius flow. The configuration and orientation of the incipient hairpin-like vortex is illustrated in terms of the concentration region of its spanwise vorticity component. Fig. 3 is a perspective view of such a vortical region and Fig. 4 is essentially a front view of the same structure. It is noted here that only one leg of the hairpin vortex is plotted in these figures, a complete haipin-like structure can be pictured by invoking the symmetrical conditions in the spanwise direction (see Fig. 1.).

Fig. 5 shows the contour surface of the streamwise velocity at t = 0. The contour level equals 0.501 and is plotted as the top surface of the depicted solid. Below this surface, the streamwise velocity has a value smaller than the contour level. The wavy part of the surface indicates the existence of retarded flow caused by the imposed hairpin vortex. It should be noted that the region depicted in Figs. 5 and 6 is only a part of the entire computational domain. Fig. 6 illustrates the contour surface of the streamwise velocity at t = 0.11. The contour level is the same as before. As it can be seen, the wavy surface spreads into the downstream region. This phenomenon is associated with the convecting hairpin vortex and the stability characteristics of the background flow. In order to further illustrate the flow patterns and dynamical processes which are currently and locally active in the observed wavy region, a sectional cut is made (section AA). This is a plane normal to the streamwise direction and close to, but in the downsteam of the tip of the initially imposed hairpin vortex.

Prior to presenting these contour plots and vector plots, it is necessary to point out the drawing scales used to produce these figures. For vector plots, the lengths of the vectors in a plane are scaled with the length of the maximum vector in that plane and at that instant. Since the maximum vector varies from plane to plane and also varies from time to time, caution should be excerised when comparing two related vector plots. In regard to the contour plots, ten levels labeled from 0-9 are used. Solid lines are used for positive values and dotted lines are used for negative values. The contour lines labeled from 0-4 are associated with f_{max}, and the lines labeled from 5-9 are associated with f_{min}, where f represents any plotted quantity. The

specific contour value associated with each line is determined by the following scheme:

	0	1	2	3	4
$f_{max} > 0$	$0.1\ f_{max}$	$0.3\ f_{max}$	$0.5\ f_{max}$	$0.7\ f_{max}$	$0.9\ f_{max}$
$f_{max} < 0$	$1.1\ f_{max}$	$1.4\ f_{max}$	$2.0\ f_{max}$	$3.3\ f_{max}$	$10.0\ f_{max}$

	5	6	7	8	9
$f_{min} > 0$	$1.1\ f_{fmin}$	$1.4\ f_{min}$	$2.0\ f_{min}$	$3.3\ f_{min}$	$10.0\ f_{min}$
$f_{min} < 0$	$0.1\ f_{min}$	$0.3\ f_{min}$	$0.5\ f_{min}$	$0.7\ f_{min}$	$0.9\ f_{min}$

Obviously, both f_{max} and f_{min} vary from plane to plane and also vary from time to time. Again, caution should be exercised when comparing two related contour plots. Although this choice of drawing scales may appear inconvenient when compared to the use of permanently fixed contour levels and vector length, this choice can expose flow patterns and dynamical processes which are currently and locally active and, therefore, has a definite benefit for the present investigation.

All the following results are presented for a particular plane normal to the streamwise direction, i.e., section AA in Figs. 5 and 6. The orientation of these figures is with respect to a viewer located in the downstream region of this plane while looking toward the upstream direction. Fig. 7 shows the cross-flow pattern at t = 0, and Fig. 8 illustrates the distribution of streamwise velocity at this instant. Although there is a sweep-like motion, it is very weak (qmax = 0.009), and the flow essentially remains to be the Blasius flow. This can also be seen from Figs. 9 and 10, which indicate that the vorticity field is almost solely composed of layers of spanwise vorticity

component. In the course of the time, the flow in this plane will evolve under the influences of a convecting hairpin-like vortex and the stability characteristics of the local, instantaneous flow. The following figures illustrate the results obtained for t = 0.11.

Fig. 11 shows the cross-flow pattern at this instant. First of all, there exists an appreciable streamwise vortex. Secondly, near the center plane (left boundary of the plot), the flow exhibits a relatively strong ejection-like motion. For the purpose of describing the spatial distribution of a flow quantity with respect to this vortex, a schematic of this cross-flow pattern is always given in the following analysis. The streamwise velocity is shown in Fig. 12. The contour lines exhibit appreciable undulations, which indicate that, roughly speaking, the flow is retarded in region A while accelerated in region B.

The rotational state of the fluid particles at this moment is indicated in Fig. 13 (projected vorticity field) and Fig. 14 (the streamwise vorticity component). As shown in Fig. 13, both the ejection and vortex regions display an appreciable amount of normal vorticity and intensified spanwise vorticity. However, the vorticity in region S is depleted when compared with the background value. The contour pattern of the streamwise vorticity is shown in Fig. 14. This pattern coincides well with the revolving cross-flow shown in Fig. 11. Fluid particles very close to the wall possess significant streamwise vorticity with a sign being opposite to that in the vortex region. From Figs. 13 and 14, it is clear that the helical vortex is associated with a strongly three-dimensional vorticity field.

Up to this point, the analysis has been focused upon the kinematics of the flow. In order to understand the dynamics of the flow, quantities which represent the production/depletion of linear and angular momentum associated with fluid particles must be investigated. The three-dimensional vorticity transport equations indicate that, for nearly incompressible flow with constant dynamic viscosity, there are two mechanisms responsible for the change of vorticity. The first one is the production of vorticity due to straining (i.e. deformation), and the second one is the transfer of vorticity due to viscous diffusion. It should be noted that, for two-dimensional flows, the mechanism associated with straining does not exist and the ability to simulate this mechanism is a major impetus for three-dimensional simulations such as that performed here. In the following, the currently and locally active dynamical processes associated with the production/transfer of vorticity will be discussed.

For spanwise vorticity, the production due to straining is shown in Fig. 15 while the transfer due to viscous diffusion is given in Fig. 16. Keeping in mind that the spanwise vorticity has negative values, Fig. 15 indicates that the straining mechanism tends to decrease the intensity of the spanwise vorticity in the vortex core region. However, this process is much more active around the peripheral than in the vortex core. The straining mechanism is most active in the ejection-like region in which the spanwise vorticity strength tends to be largely increased. Below this ejection-like region, the straining mechanism tends to deplete the local spanwise vorticity. From Fig. 16, it can be seen that the a roof-shaped region extends from the ejection region to the vortex core and the viscous diffusion process is quite active inside this layer of fluid; the strength of the spanwise vorticity tends to be decreased in this layer. The viscous diffusion process is not active around most of the vortex peripheral region. In the corner formed by the center plane and the wall, the spanwise vorticity is being intensified by viscous diffusion. Roughly speaking, the combined effect of the straining and viscous diffusion processes is to increase the strength of spanwise vorticity in the ejection region and to decrease the intensity of spanwise vorticity in the vortex core region. For streamwise vorticity, the production due to the straining and the viscous diffusion process is shown in Figs. 17 and 18, respectively. Inside and around the vortex core region, the straining mechanism dominates over the viscous diffusion, and its effect is to intensify the current streamwise vorticity associated with the fluid particles in this region (see Fig. 14). The effects of viscous diffusion on the transfer of streamwise vorticity are practically negligible in the vortex and ejection region. However, it is quite active in the immediate neighborhood of the wall. For normal vorticity component, the dynamical situation is shown in Fig. 19 (production due to straining) and Fig. 20 (transfer due to viscous diffusion). Both mechanisms are active inside and around the vortex core region, in particular, the region between ejection-like motion and revolving motion. Nevertheless, the effects due to the straining process are relatively stronger, resulting in an intensification of the normal vorticity (see Fig. 13 for the sign of normal vorticity in this region). Again, in a layer attached to the wall and close to the center plane (left boundary of the plot), the viscous diffusion process is also significant.

The above discussion indicates that the relative importance between the straining mechanism and the viscous diffusion mechanism in a region can depend

upon the specific vorticity component under concern. In addition, the fluid mass in the corner of the wall and the center plane is a source of dormant, upward migration. From Figs. 15-20, it can be seen that both straining and viscous diffusion processes of vorticity production are active in this region. Furthermore, the flow in this region is less dissipative than the Blasius flow. Fig. 21 illustrates the variation of dissipation per unit mass from the Blasius values. Both the vortex core and ejection region become more dissipative. However, the center plane corner region becomes less dissipative. This region is probably a part of a streamwise low-speed streak, as indicated by Figs. 11 and 22. It is noted here that Fig. 22 is a side view which displays the difference of the projected velocity vector field between the current flow and the steady Blasius flow. Since the latter contains no organized structure, this figure exposes structures embedded in a convecting flow. It can be seen that the center plane corner in Fig. 11 is a part of the retarded wall flow. In other words, this is a region in which hydrogen bubbles or dye materials will tend to accumulate in the case of flow visualization.

The above discussion focused upon the dynamical state of the angular motion of fluid particles currently in a plane normal to the streamwise direction. Also discussed is the current dissipative state of these particles. The translational motion of fluid particles is governed by the velocity transport equation, which indicates that the translational dynamics is controlled by spatial gradients of static pressure and viscous stresses. Fig. 23 shows the distribution of the static pressure coefficient. The most intense gradients occur in the ejection region which is close to the center plane and relatively far away from the wall. The vortex core region does not coincide with the low pressure center region, nor the high pressure center region, but it is located in a low pressure region. Furthermore, the pressure gradient inside the vortex core is not significant over most part of the cross-section. Consequently, the viscous stress must play an important role in sustaining such a revolving flow pattern. Fig. 24 shows the distribution of S_{yz}, which is one component of the viscous shear stress. There is a wall layer with intense shear stress, and the close-looped contour pattern coincides well with the revolving flow pattern. It is noted here that Fig. 14 and Fig. 24 are quite similar, and this is due to the large spanwise-velocity gradient in the direction normal to the wall. In contrast to the concentrated distribution of the shear stress S_{yz} inside and around the vortex core, the effects of

viscous normal stresses S_{yy} and S_{zz} are not important in this region, as can be inferred from Figs. 25 and 26. Furthermore, the effects associated with these viscous normal stresses are practically negligible when compared with the effects due to static pressure. This is also the case for S_{xx} (Fig. 27), which is the normal stress acting on this plane. The shear stresses acting on this plane are S_{xz} (Fig. 28) and S_{xy} (Fig. 29). These two figures indicate the existance of a wedge-shaped shear layer extending from the ejection region to the vortex core region. This is better illustrated by considering the difference of the shear stress vector in this plane between the current flow and the Blasius flow (Fig. 30). In addition to the wedge-shaped shear layer, there is an oppositely sheared region in the corner close to the centerplane. The cross-flow rushes through the alley in between these oppositely sheared regions.

The above kinematic and dynamic analyses focused upon the flow in a plane and at a given instant. Thus, it is an instantaneous and local analysis. By compiling the results derived from such an analysis, also with the aid of complementary Lagrangian and Topological analyses, the temporal evolution of the global flow field can be examined in a systematic and relatively detailed fashion. The temporal and global analysis focuses upon the identification of the common denominators appearing in the observed events, so that the underlying physical mechanisms can be investigated and better understood. For cyclic processes and the evolution of organized structures, phase-aligned comparisons will be performed. At the present time, both the numerical simulation and the accompanying data analysis are in progress. A comprehensive description of the results and their interpretation will be presented in the Final Report.

VIII. PERSONNEL

The major effort of this contract has been provided by Drs. Nan-Suey Liu, Stephen J. Shamroth, Henry McDonald and Farhad Davoudzadeh of Scientific Research Associates, Inc.

IX. CONCLUDING REMARK

It is now widely recognized that hairpin vortices are the predominant structures in the near-wall region of turbulent boundary layers. Their role in the cyclic production of wall turbulence has been studied in many laboratory experiments primarily using flow visualization techniques. Being the tractable part of wall turbulence, these organized structures may contain most of the essential physics of the turbulent boundary layers. Thus, better understanding of the dynamical significance of hairpin vortices in boundary layers is not only important to unveil the physics of turbulence per se, it also holds the key to the management and control of turbulence, which is of significant technological importance.

The study of hairpin vortices in a fully turbulent environment is greatly complicated by the presence of jitters and a large number of other structures simultaneously present in the flow. Nevertheless, there is experimental evidence which indicates that a viable way to gain better understanding of the physical processes is to study the flow dynamics stimulated by synthetically generated hairpin vortices in initially laminar boundary layers. The goal of the present effort is to describe the behavioral characteristics of the flow events/organized structures and to identify the underlying physical processes stimulated by hairpin vortices in developing boundary layers through the direct solution of time-dependent, three-dimensional, compressible Navier-Stokes equations.

The simulations in the present effort are time-marching spatial simulations for boundary layer flows. This differs from temporal simulations for plane channel flows using spectral methods. In addition, the numerical scheme used in the present effort allows the investigations of pressure gradient and compressibility effects. Three distinct but related methods of data analysis are being employed to evaluate the data provided by the numerical simulations. These methods are Eulerian analysis, Lagrangian analysis and Topological analysis. The results obtained from these analyses will be coordinated to elucidate the flow characteristics and to extract the underlying dynamics.

The results presented in this Annual Report are the kinematical and dynamical states of the flow in a plane normal to the streamwise direction at a given instant. The spatial distributions of various flow quantities over a

cross-section of the streamwise vortex have been examined and interpreted. These quantities are translational velocity, vorticity, production of vorticity due to straining, viscous diffusion of vorticity, dissipation, static pressure and viscous stress tensor. Such instantaneous, local analysis, together with complementary Lagrangian and Topological analyses, will yield a temporal and global analysis aimed at providing more insight into the cyclic turbulence production and transport processes in turbulent flows. The focus of the future work is to carry out this ongoing simulation and the accompanying data analysis.

REFERENCES

[1] Hussain, A.K.M.F.: Coherent Structures and Turbulence. J. Fluid Mech., Vol. 173, pp. 303-356, 1986.

[2] Talmon, A.M., Kunen, J.M.G. and Ooms, G.: Simultaneous Flow Visualization and Reynolds-Stress Measurement in a Turbulent Boundary Layer. J. Fluid Mech., Vol. 163, pp. 459-478, 1986.

[3] Leonard, A.: Vortex Methods for Flow Simulation. J. Comput. Physics, Vol. 37, pp. 289-335, 1980.

[4] Ersoy, S. and Walker, J.D.A: The Viscous Flow Induced Near a Wall by Counter-Rotating Vortex Pairs and Vortex Loops. AFOSR Report FM-8, 1985.

[5] Biringen, S.: Three-Dimensional Vortical Structures of Transition in Plane Channel Flow, AIAA-87-0046, AIAA 25th Aerospace Sciences Meeting, 1987.

[6] Singer, B.A., Ferziger, J.H. and Reed, H.L.: Effect of Streamwise Vortices on Transition in Plane-Channel Flow. AIAA-87-0048, AIAA 25th Aerospaces Sciences Meeting, 1987.

[7] Moin, P.: Analysis of Turbulence Data Generated by Numerical Simulations. AIAA-87-0194, AIAA 25th Aerospace Sciences Meeting, 1987.

[8] Head, M.R. and Bandyophadyay, P.: New Aspects of Turbulent Boundary-Layer Structure. J. Fluid Mech., Vol. 107, pp. 297-337, 1981.

[9] Perry, A.E. and Chong, M.S.: On the Mechanisms of Wall Turbulence, J. Fluid Mech., Vol. 119, pp 173-217, 1982

[10] Moin, P. and Kim, J.: The Structure of the Vorticity Field in Turbulent Channel Flow. Part 1. Analysis of Instantaneous Fields and Statistical Correlations. J. Fluid Mech., Vol. 155, pp. 441-464, 1985

[11] Acarlar, M.S. and Smith, C.R.: An Experimental Study of Hairpin-Type Vortices as a Potential Flow Structure of Turbulent Boundary Layers. AFOSR Report FM-5, 1984.

[12] Liu, N.-S., Shamroth, S.J. and McDonand, H.: On Hairpin Vortices as Model of Wall Turbulence Structure. Proc. 5th Symposium on Turbulent Shear Flow. pp. 2.1-2.6, 1985.

[13] Briley, W.R. and McDonald, H.: On the Structure and Use of Linearized Block Implicit Schemes. J. Comp. Physics, Vol. 34, pp. 54-72, 1980.

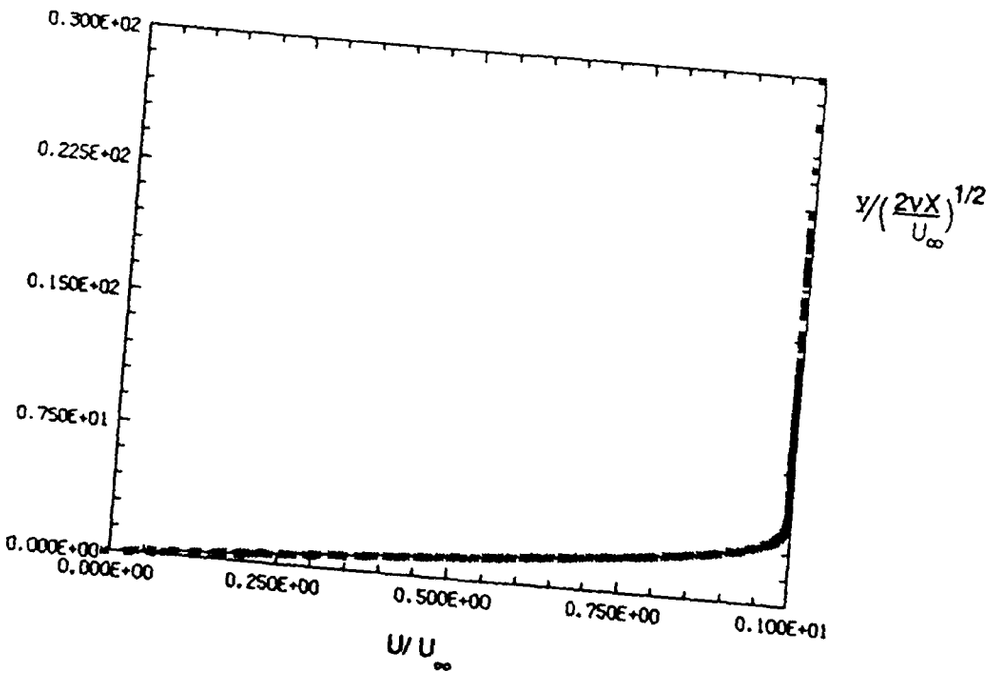

Fig. 2. Velocity profile of the background flow.
- : Blasius theory
* : Numerical solution

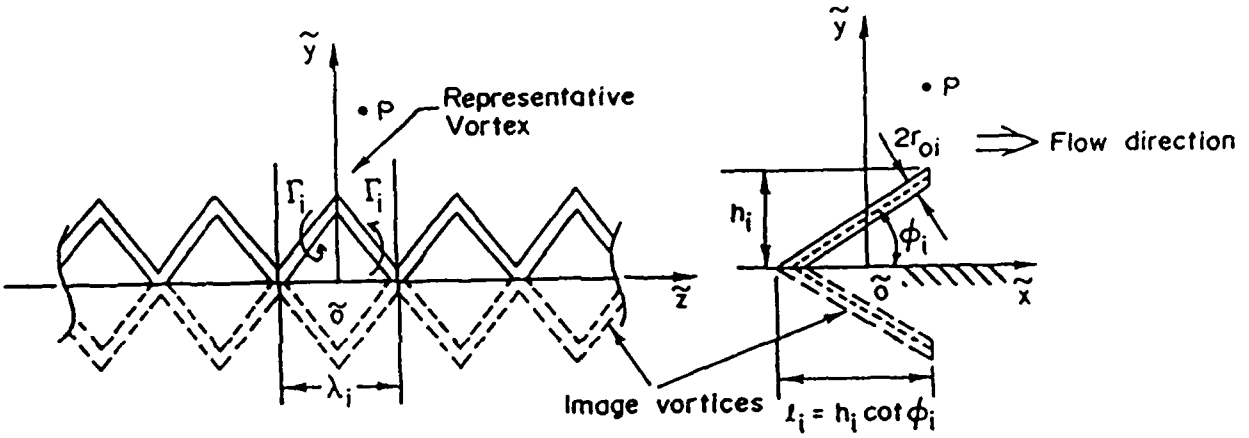

Fig. 1. A schematic of an array of hairpin vortices and representative vortex.

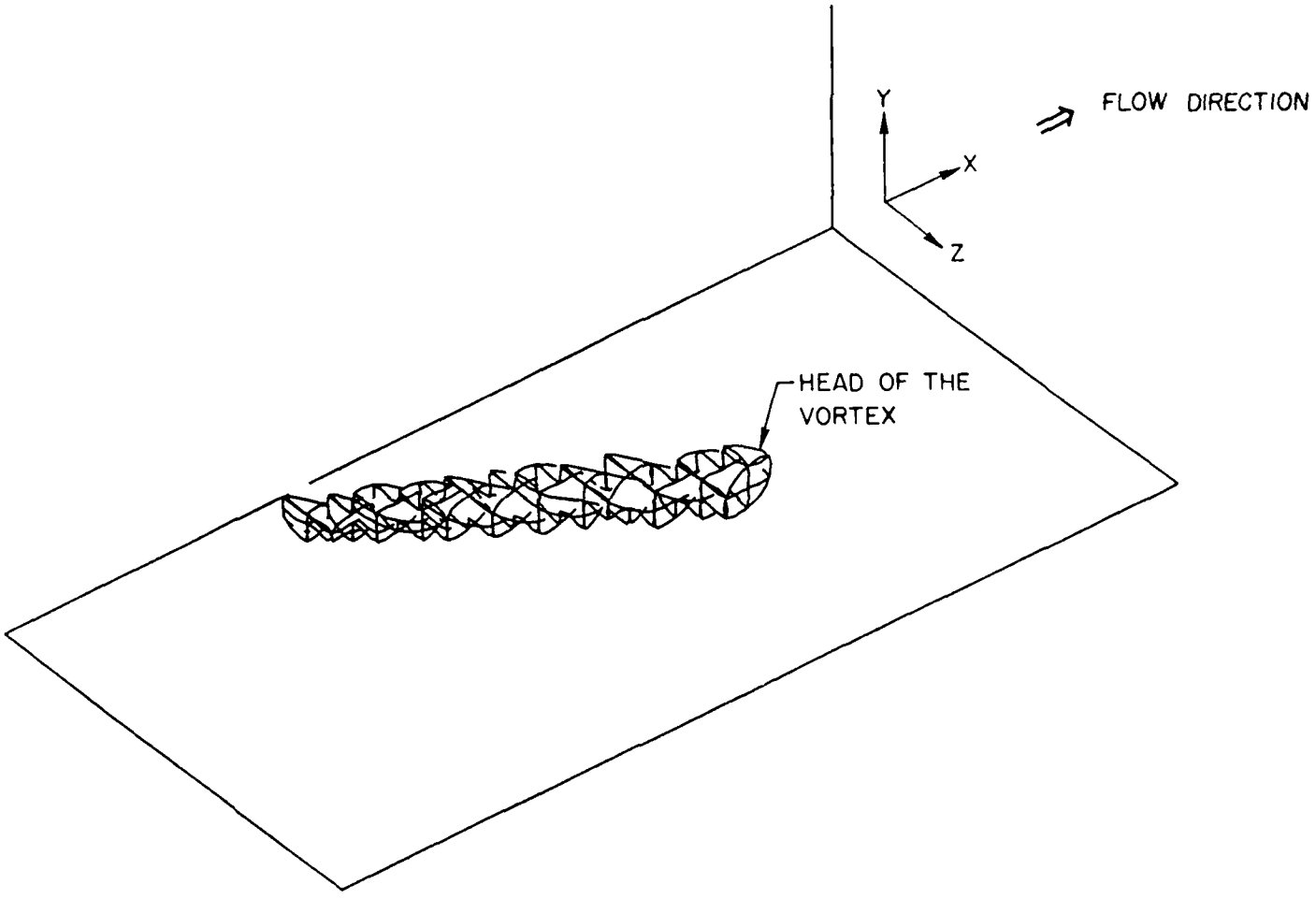

Fig. 3. Concentration of spanwise vorticity associated with the incipient hairpin vortex (only one leg is shown).

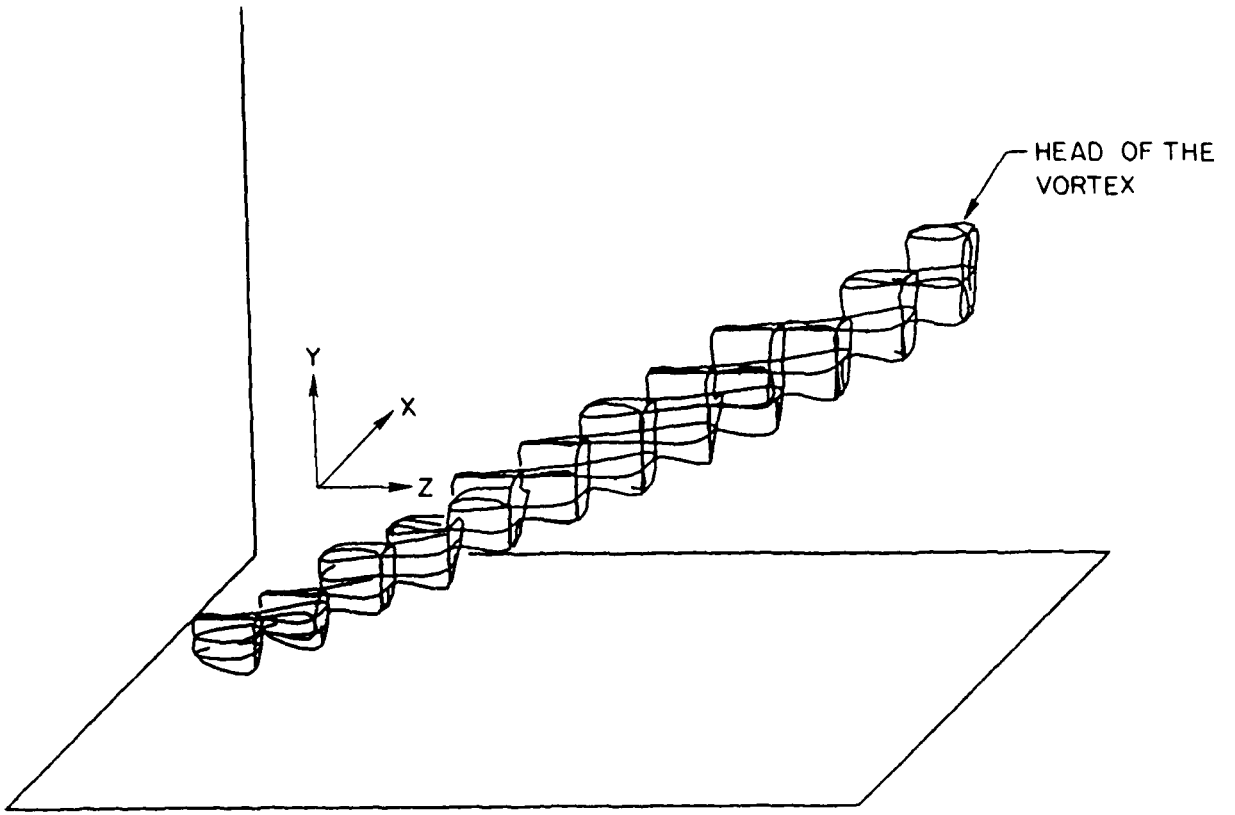

Fig. 4. Front view of the structure depicted in Fig 3.

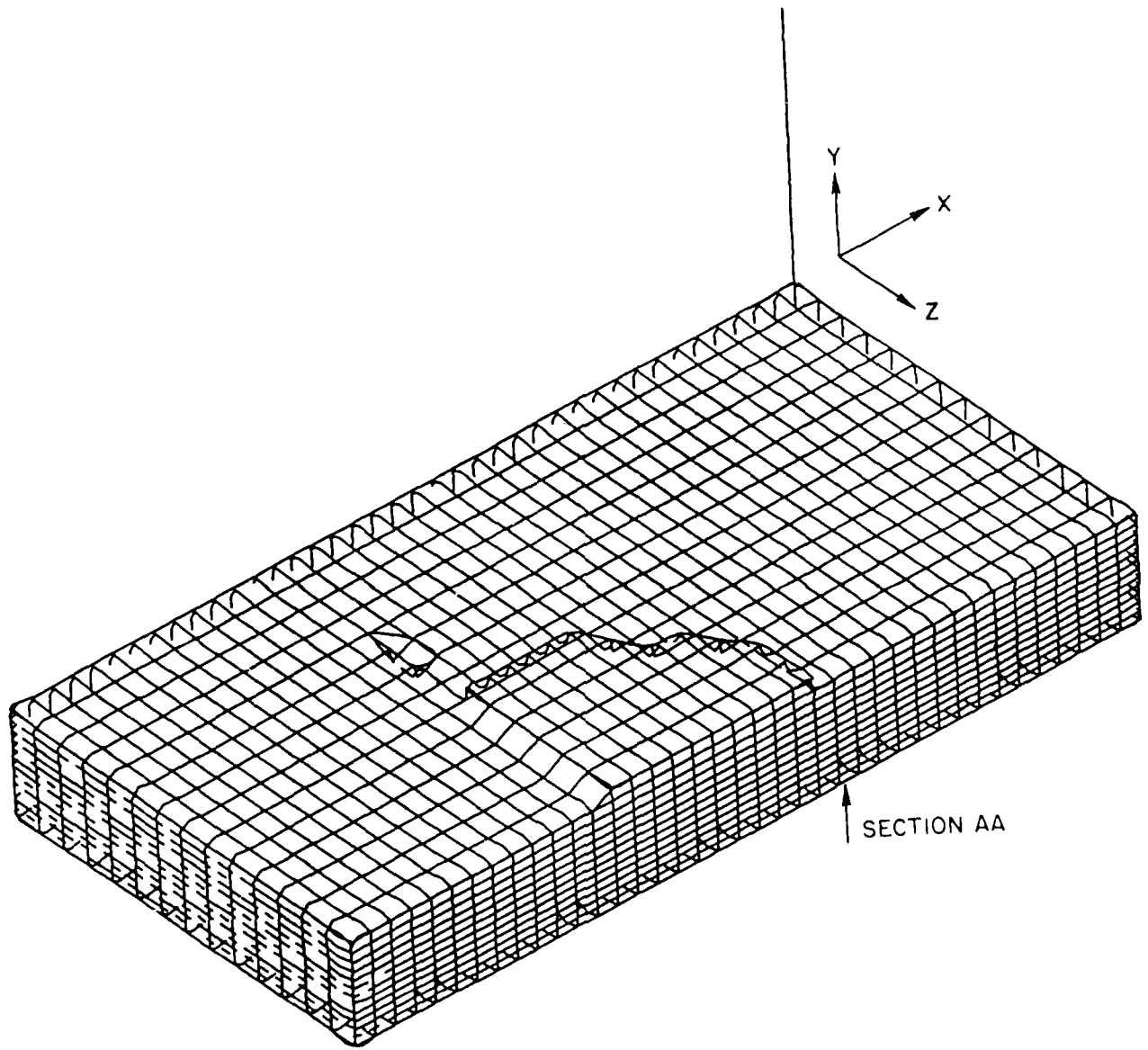

Fig. 5. Contour surface of streamwise velocity at t=0.
(Contour level is 0.501)

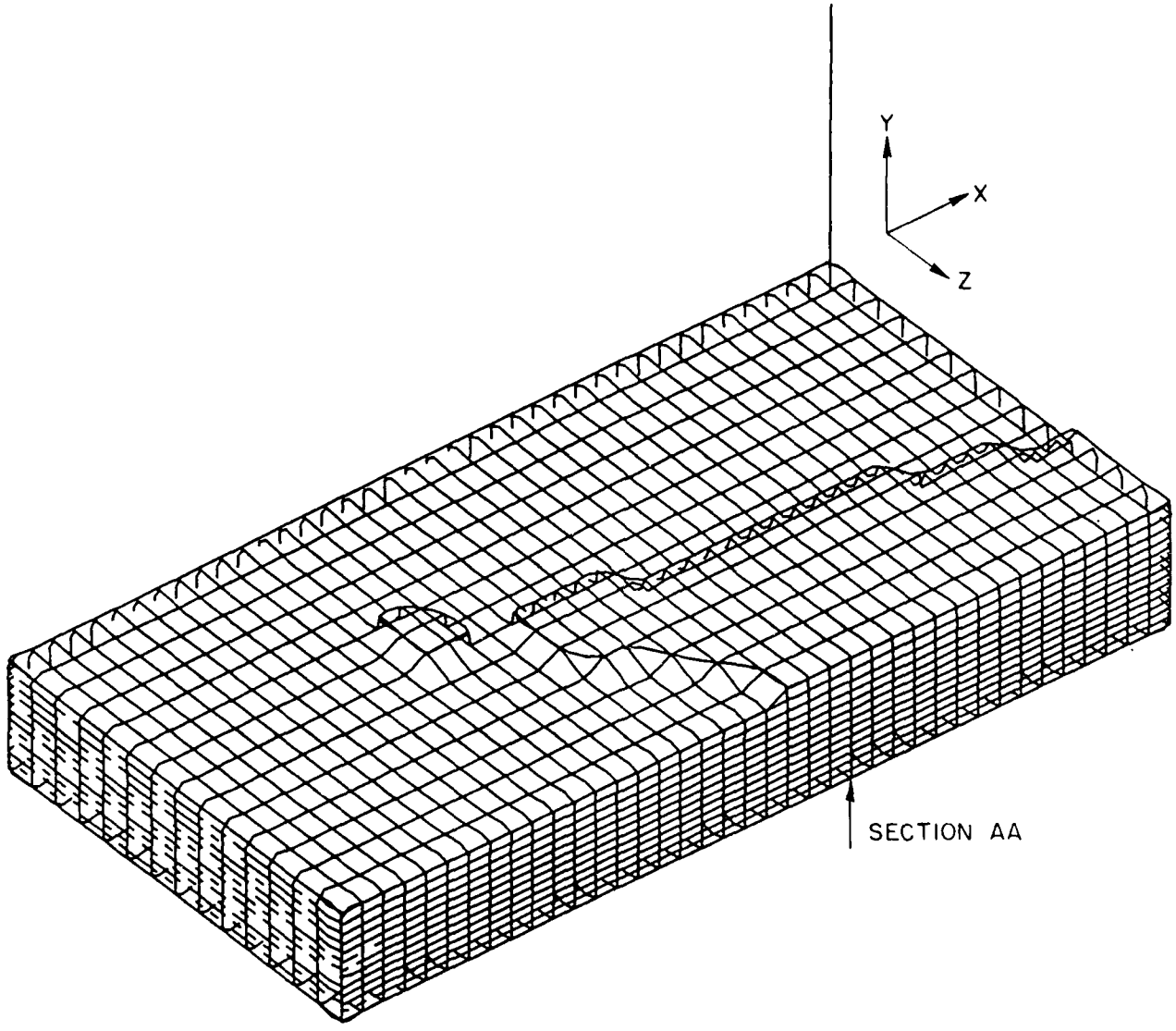

Fig. 6. Contour surface of streamwise velocity at t=0.11. (Contour level is 0.501)

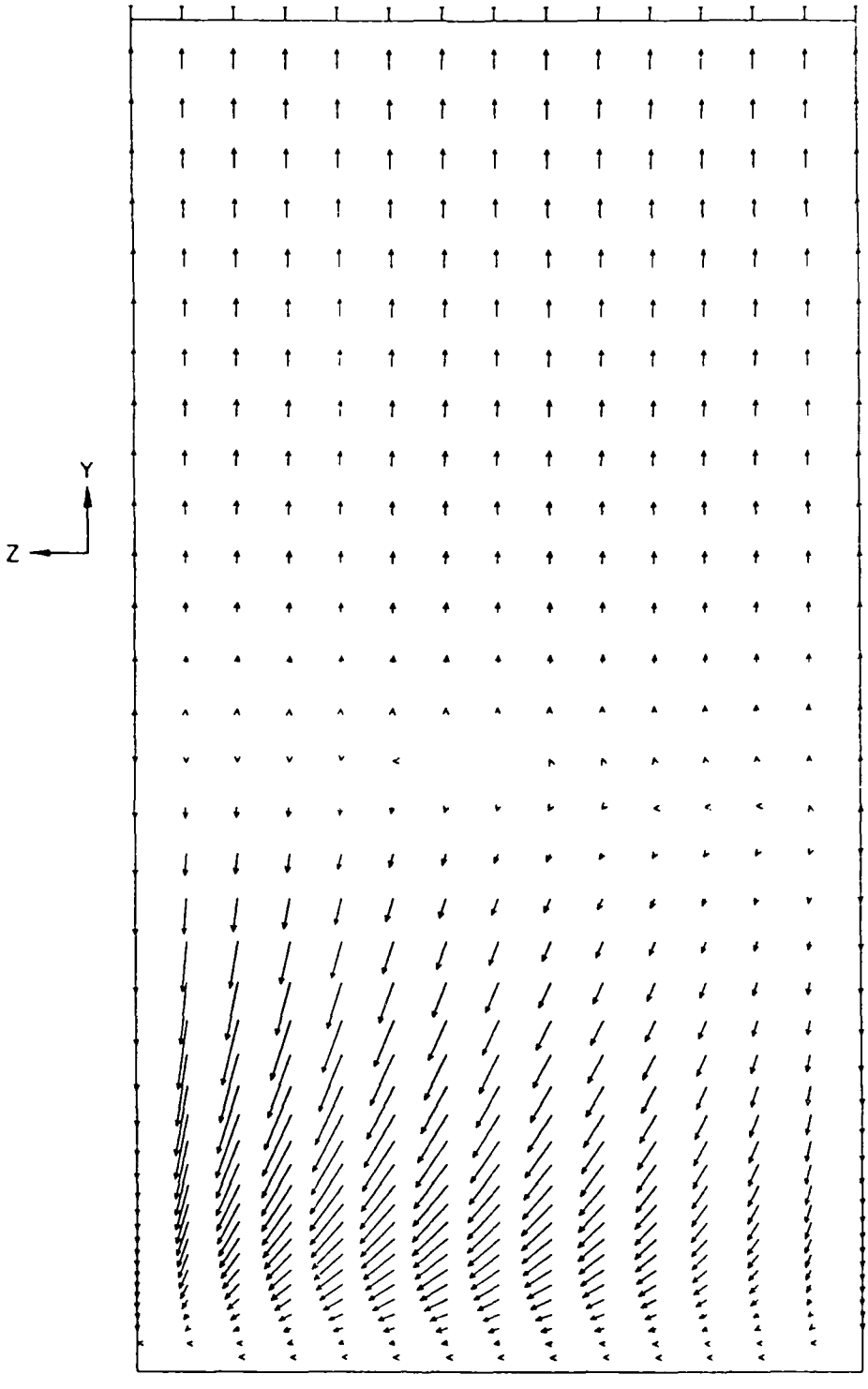

Fig. 7. Projected velocity field at t=0. (q_{max}=0.009)

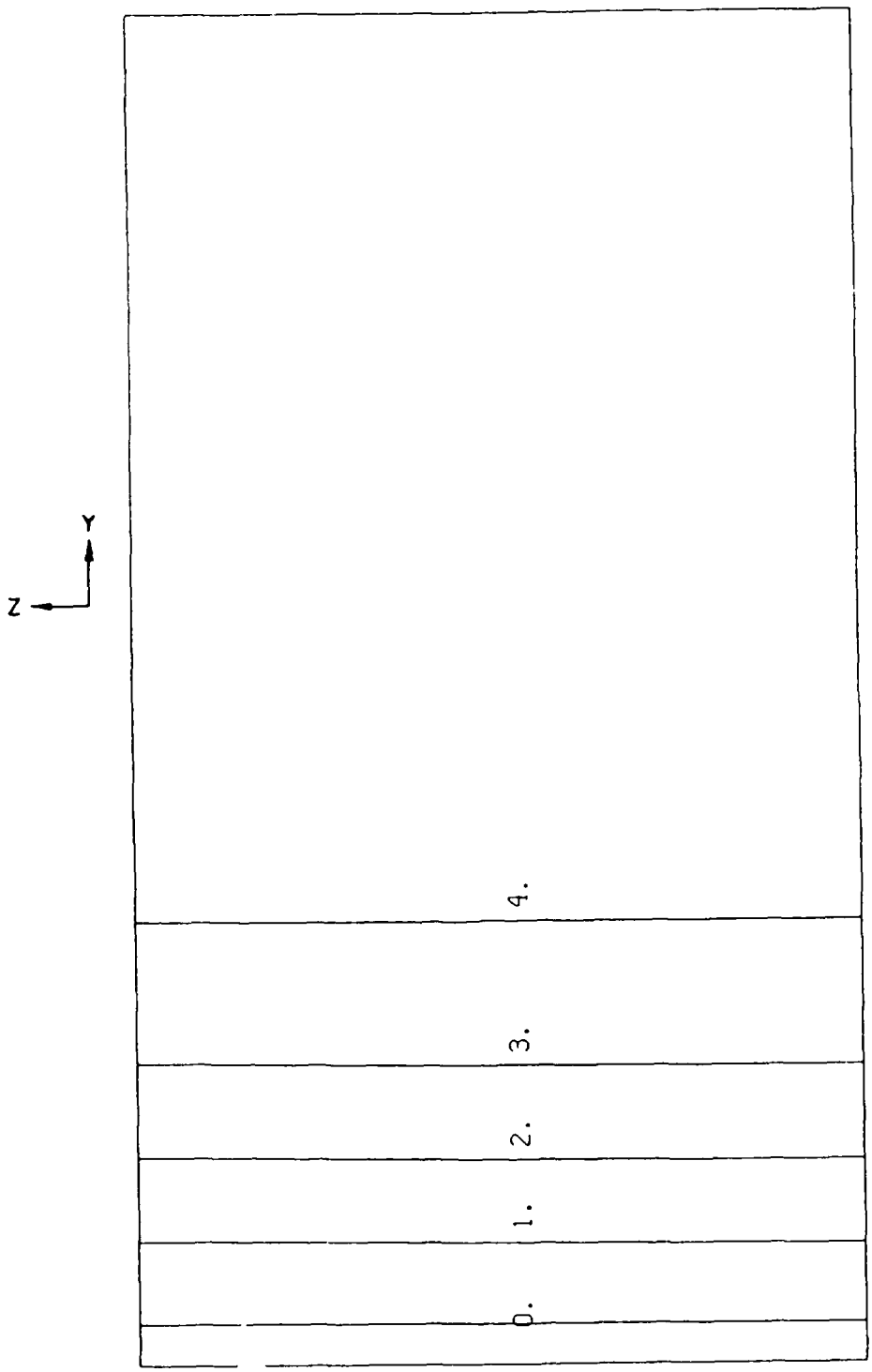

Fig. 8. Streamwise velocity at t=0.
(f_{max}=1.0017, f_{min}=0)

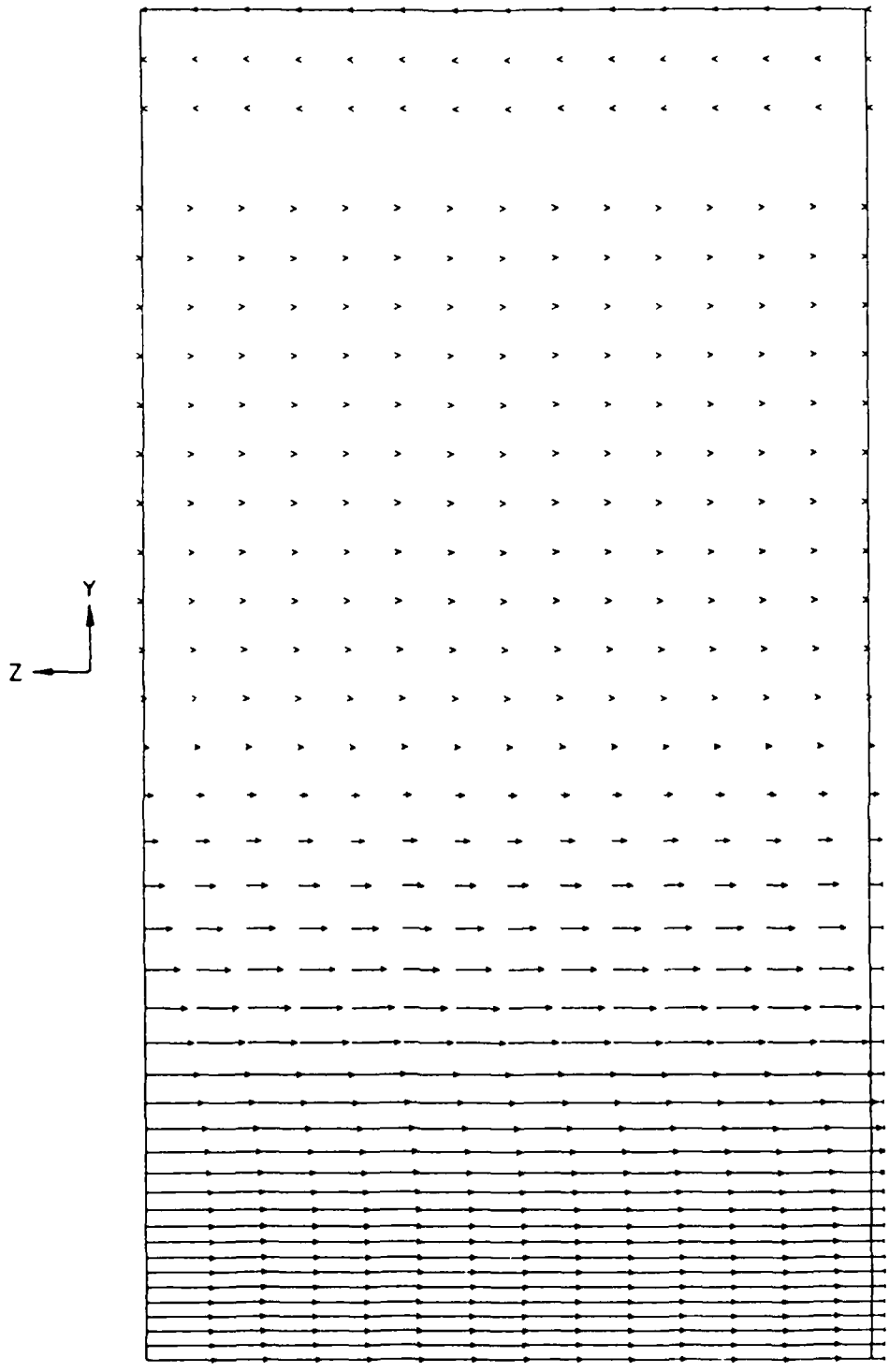

Fig. 9. Projected vorticity field at t=0.
(q_{max}=31.087)

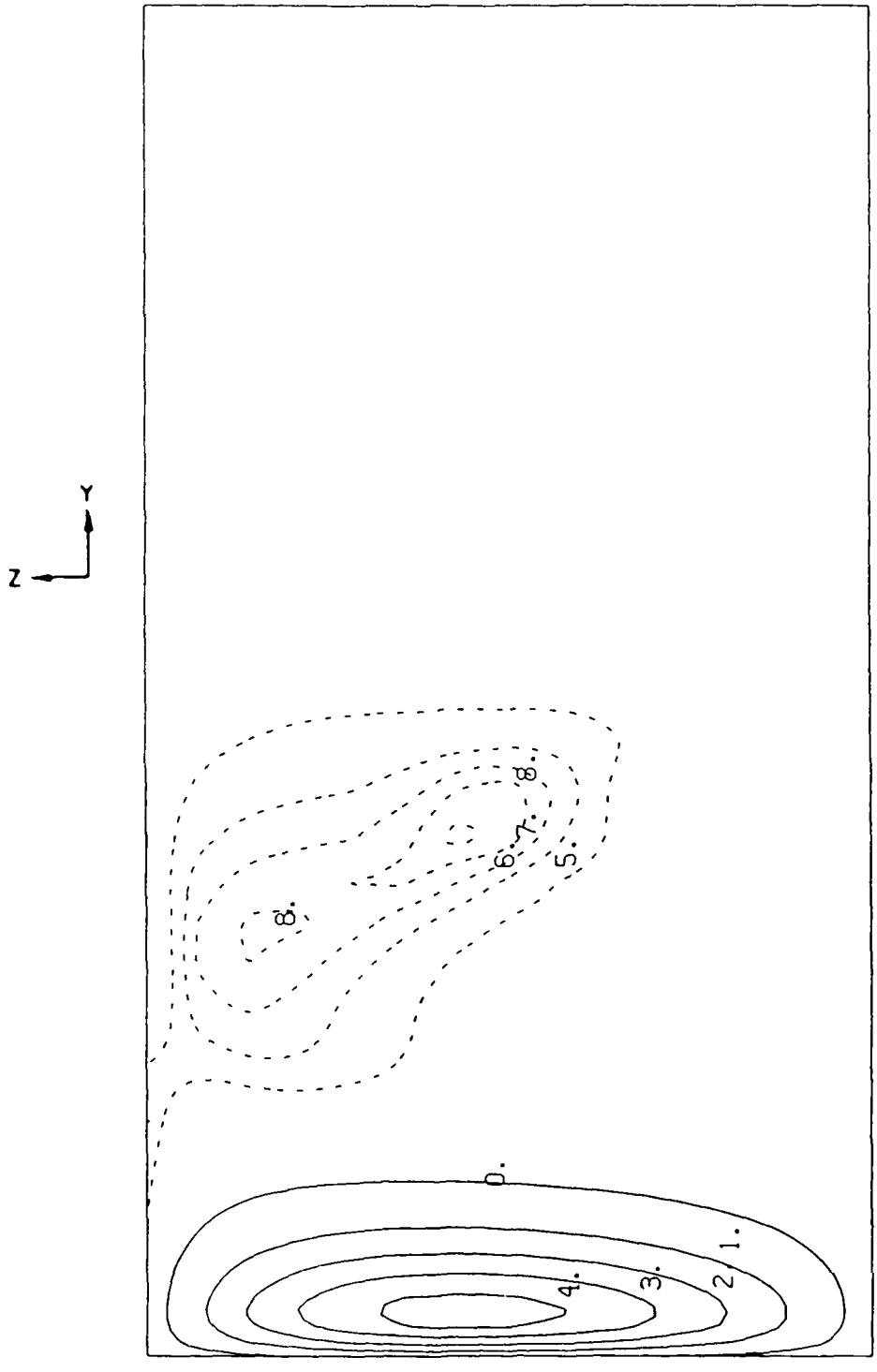

Fig. 10. Streamwise vorticity at t=0.
(f_{max}=0.6082, f_{min}=-0.0257)

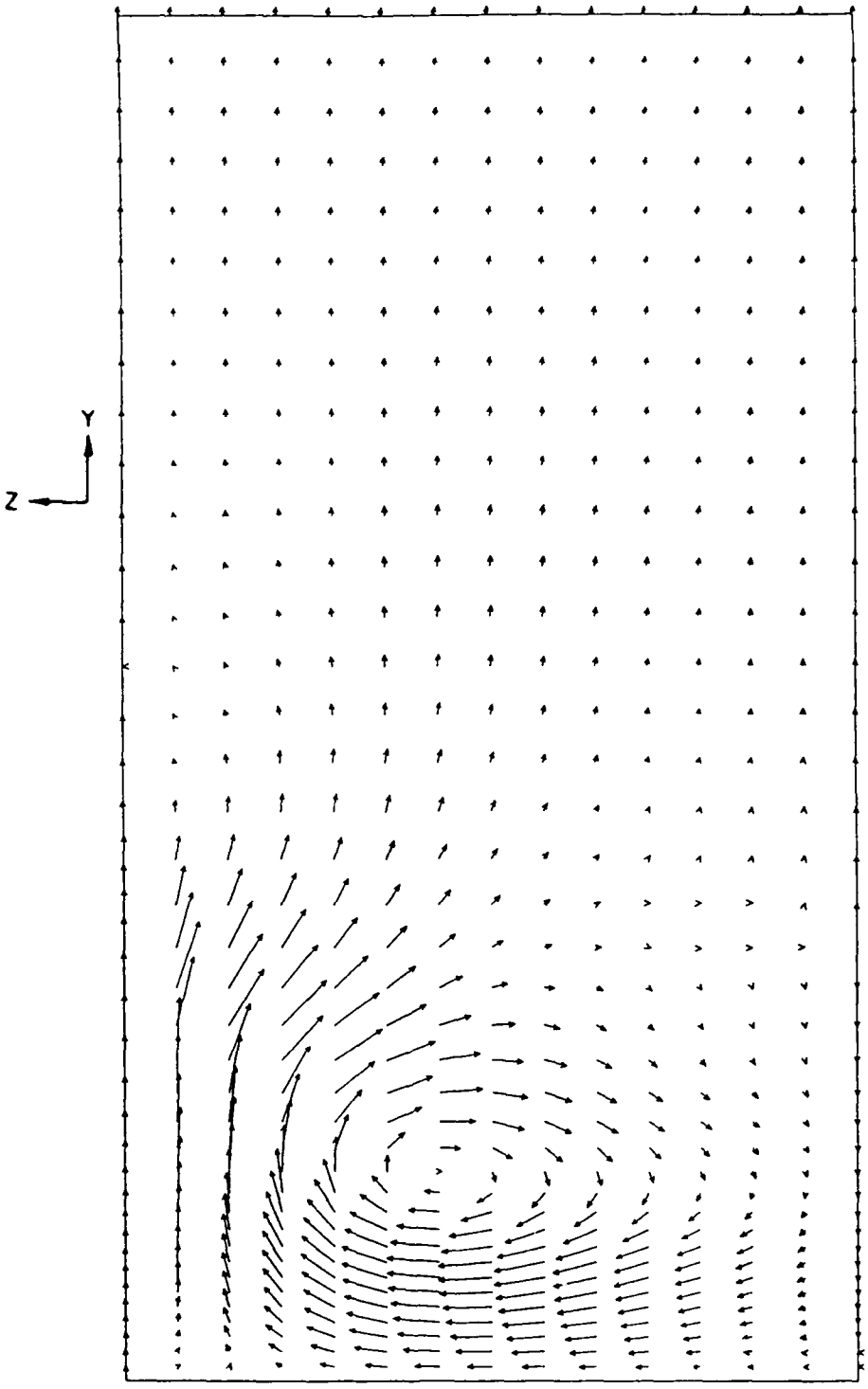

Fig. 11. Projected velocity field at t=0.11. (q_{max}=0.026)

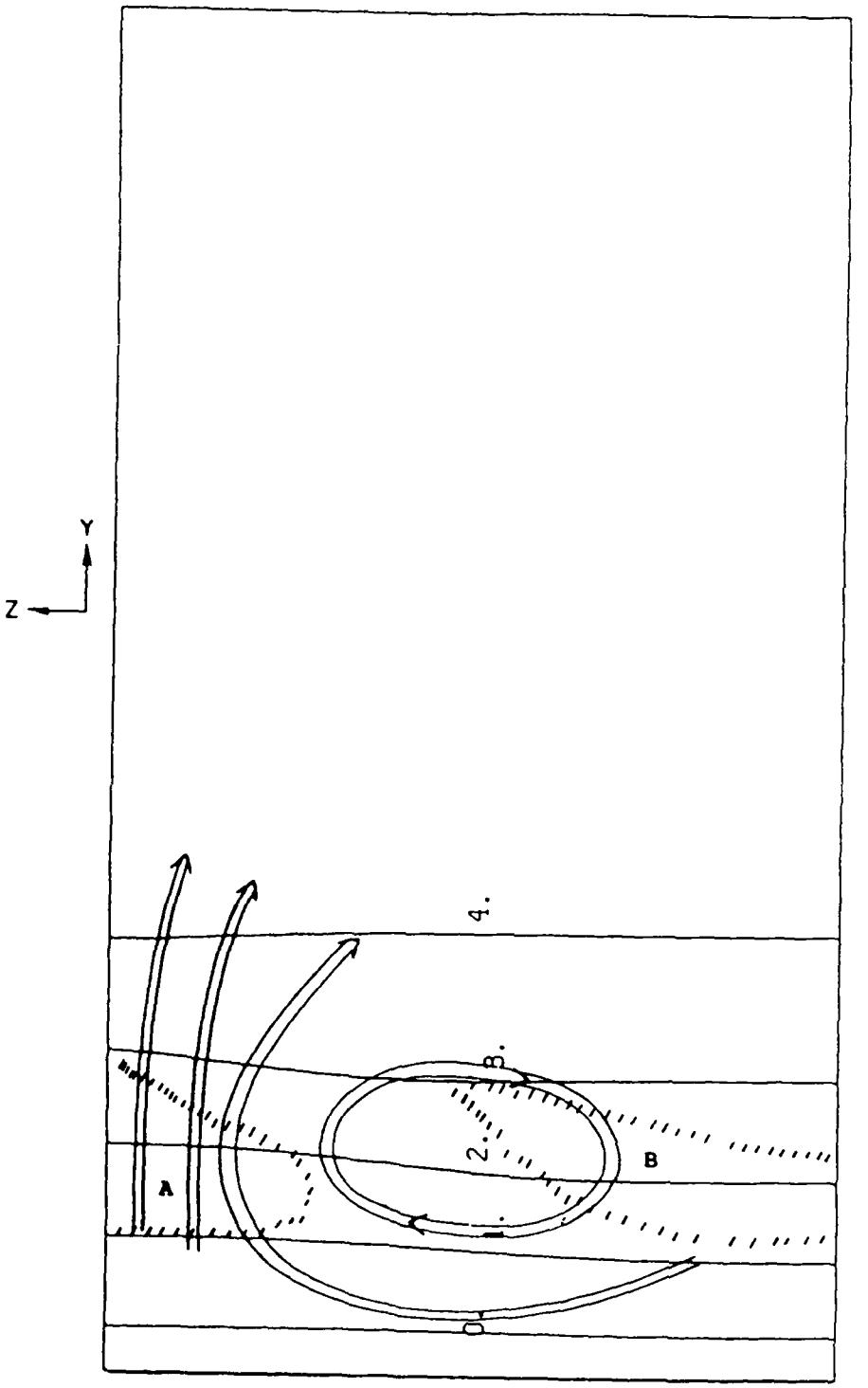

Fig. 12. Streamwise velocity at t=0.11.
(f_{max}=1.0019, f_{min}=0.0)

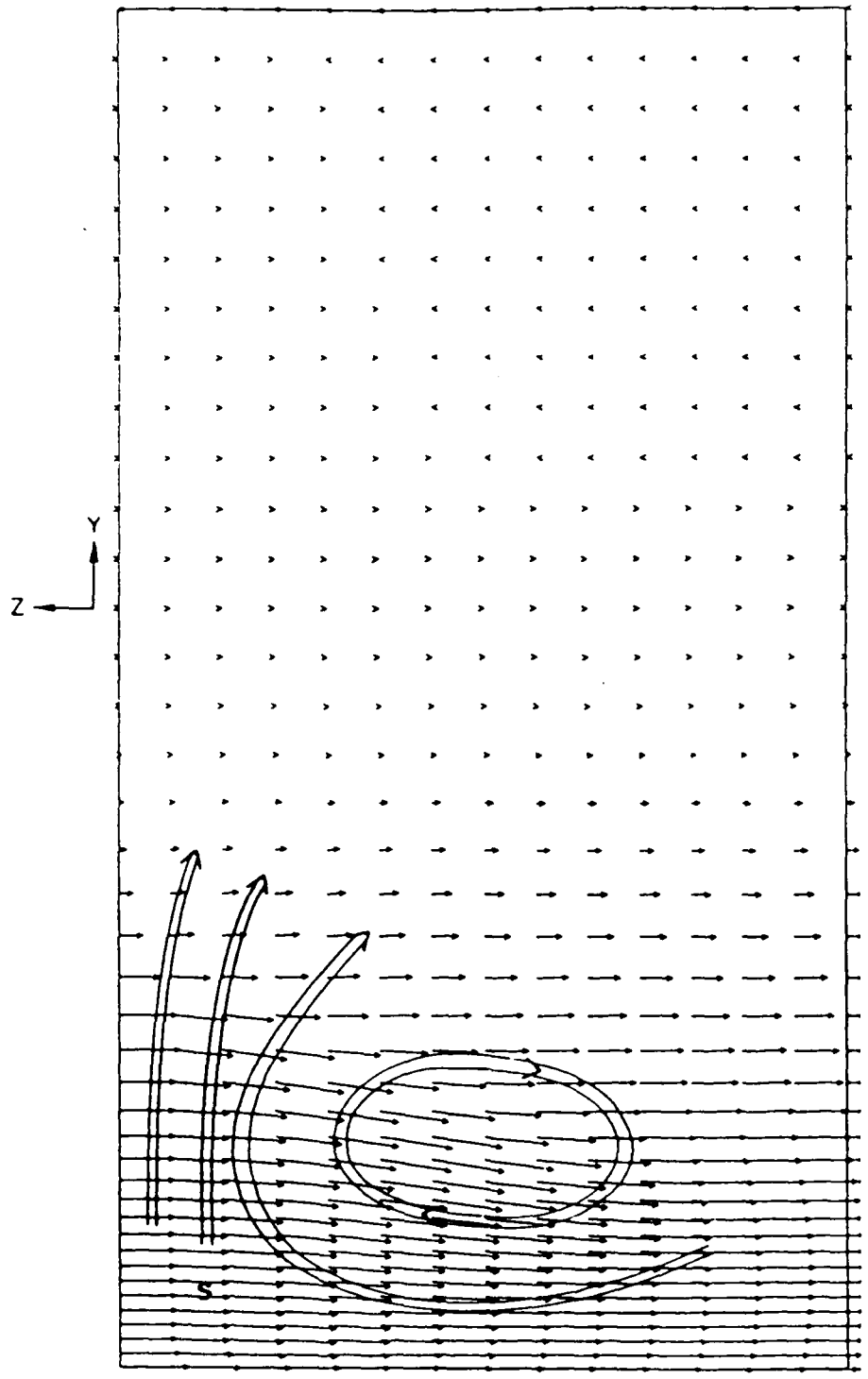

Fig. 13. Projected vorticity field at t=0.11.
(q_{max}=33.339)

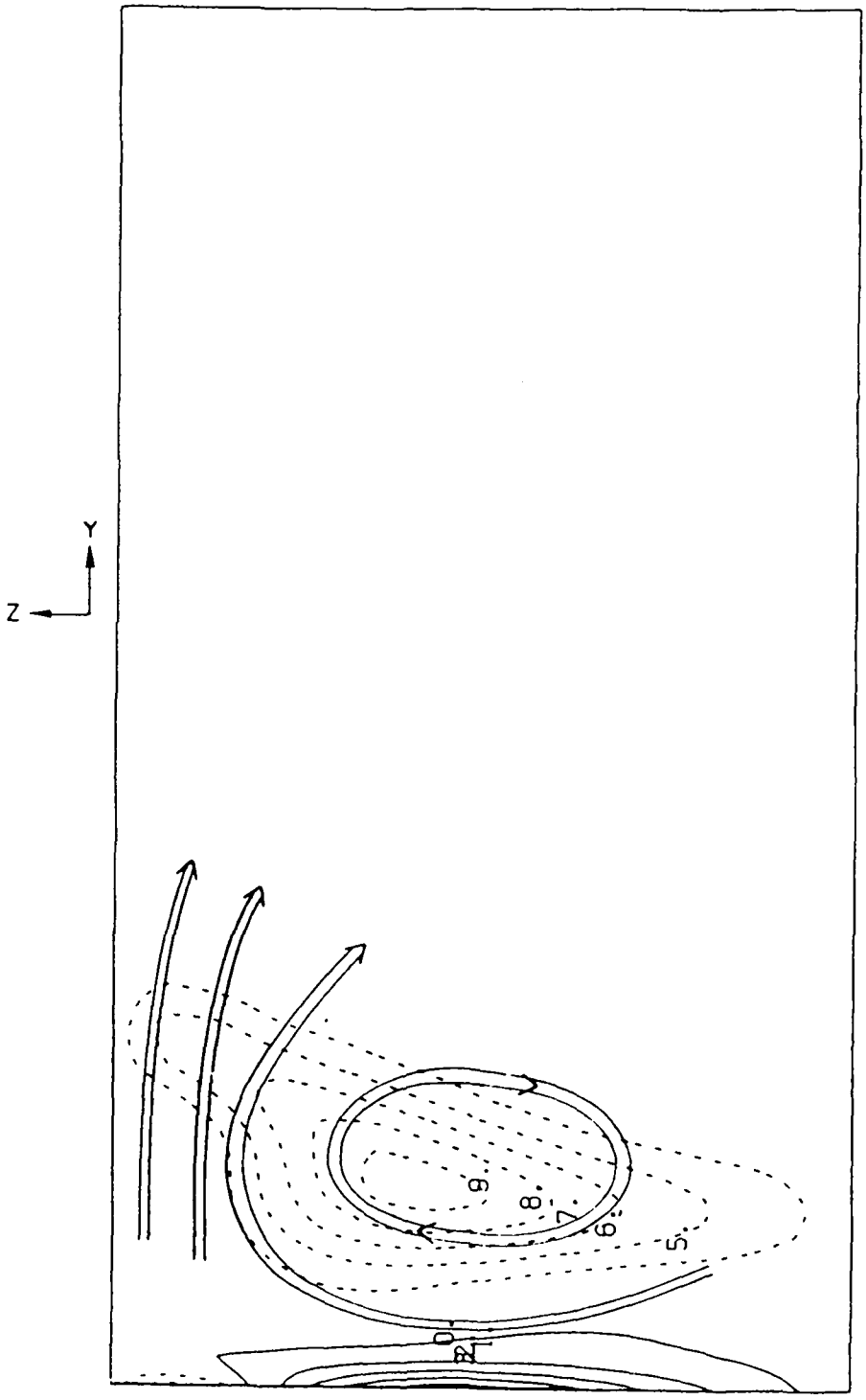

Fig. 14. Streamwise vorticity at t=0.11.
(f_{max}=9.8743, f_{min}=-4.7792)

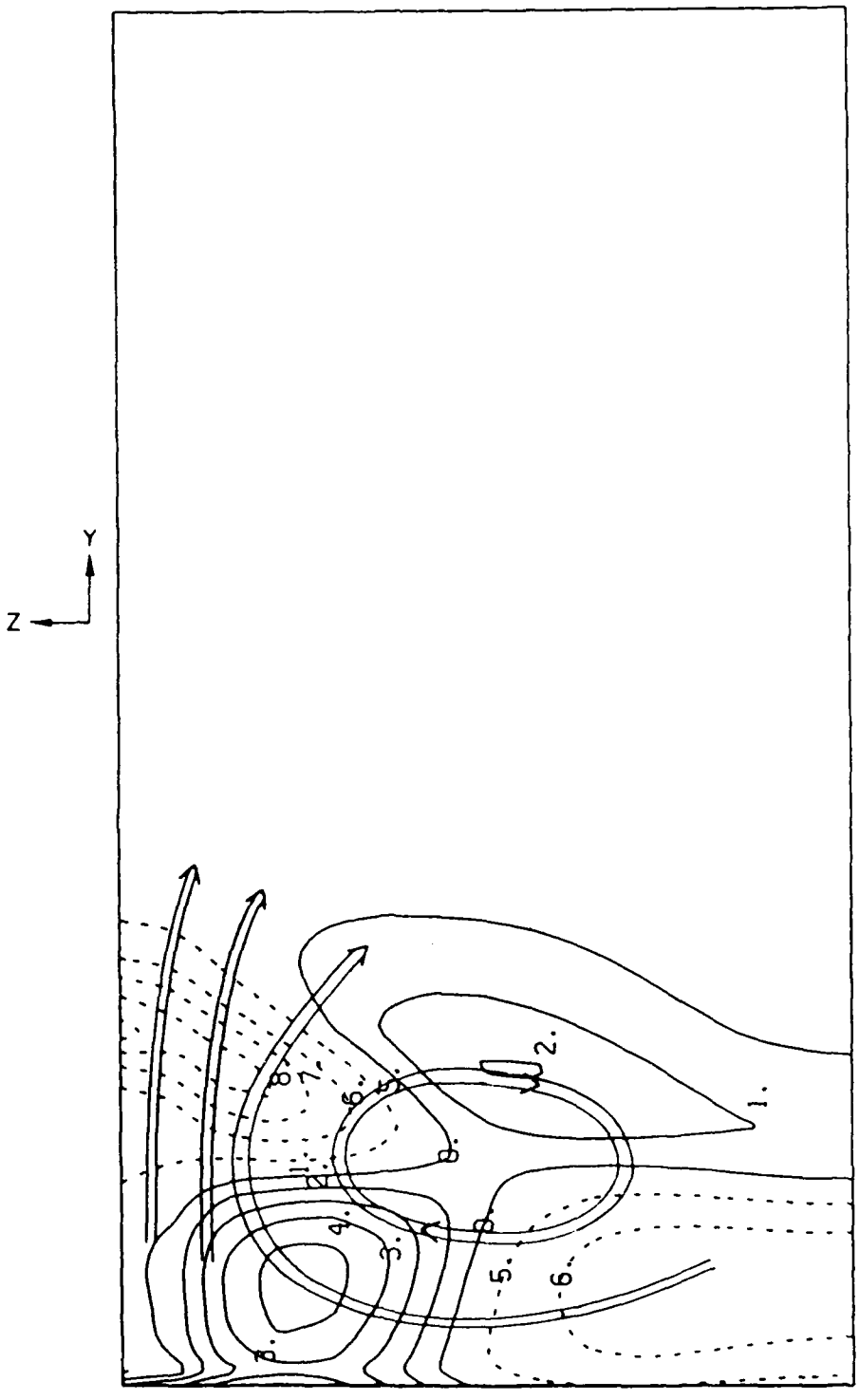

Fig. 15. Production of spanwise vorticity due to straining at t=0.11.
(f_{max}=30.5088, f_{min}=-54.0696)

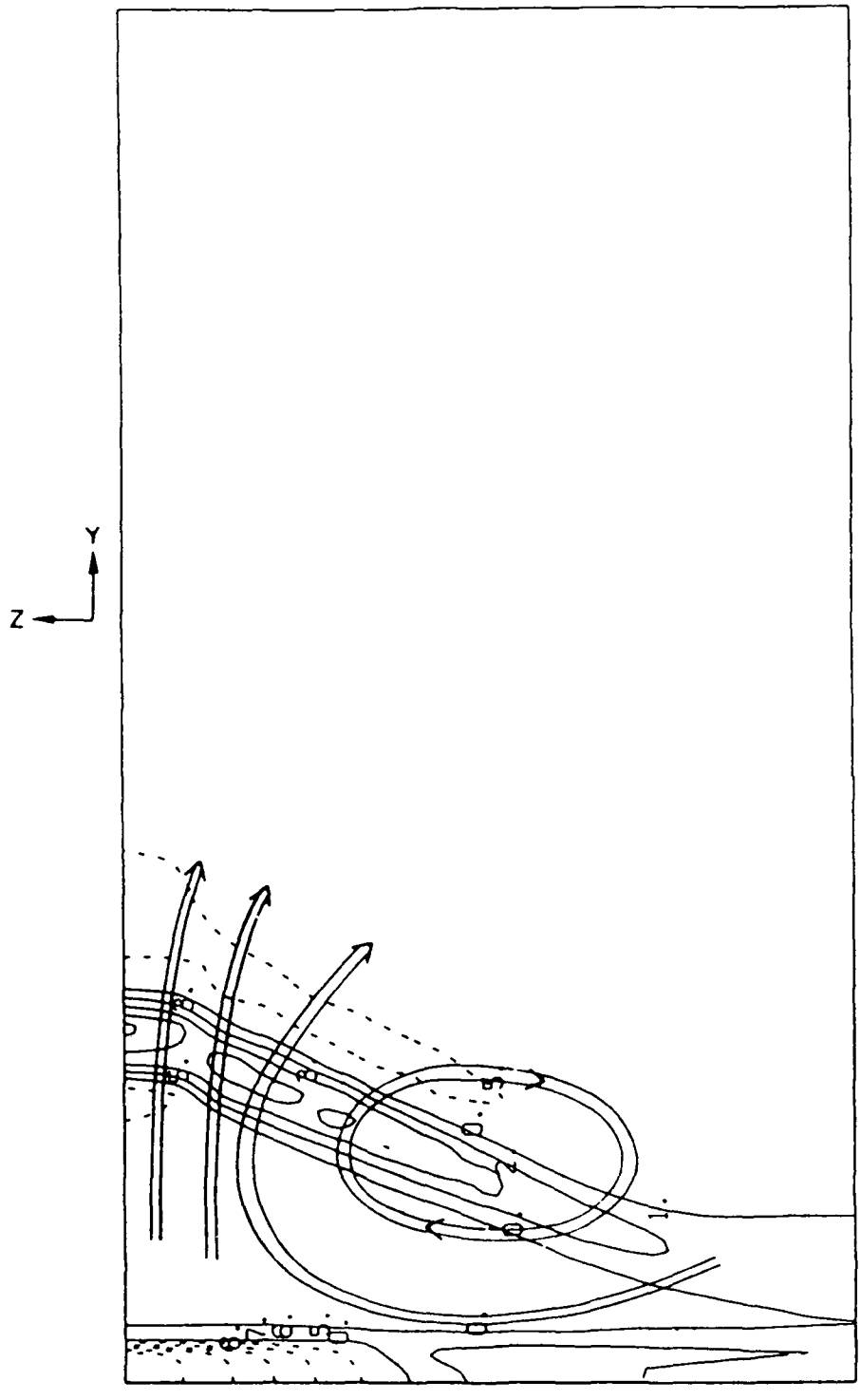

Fig. 16. Transfer of spanwise vorticity due to viscous diffusion at t=0.11. (f_{max}=32.5780, f_{min}=-56.8881)

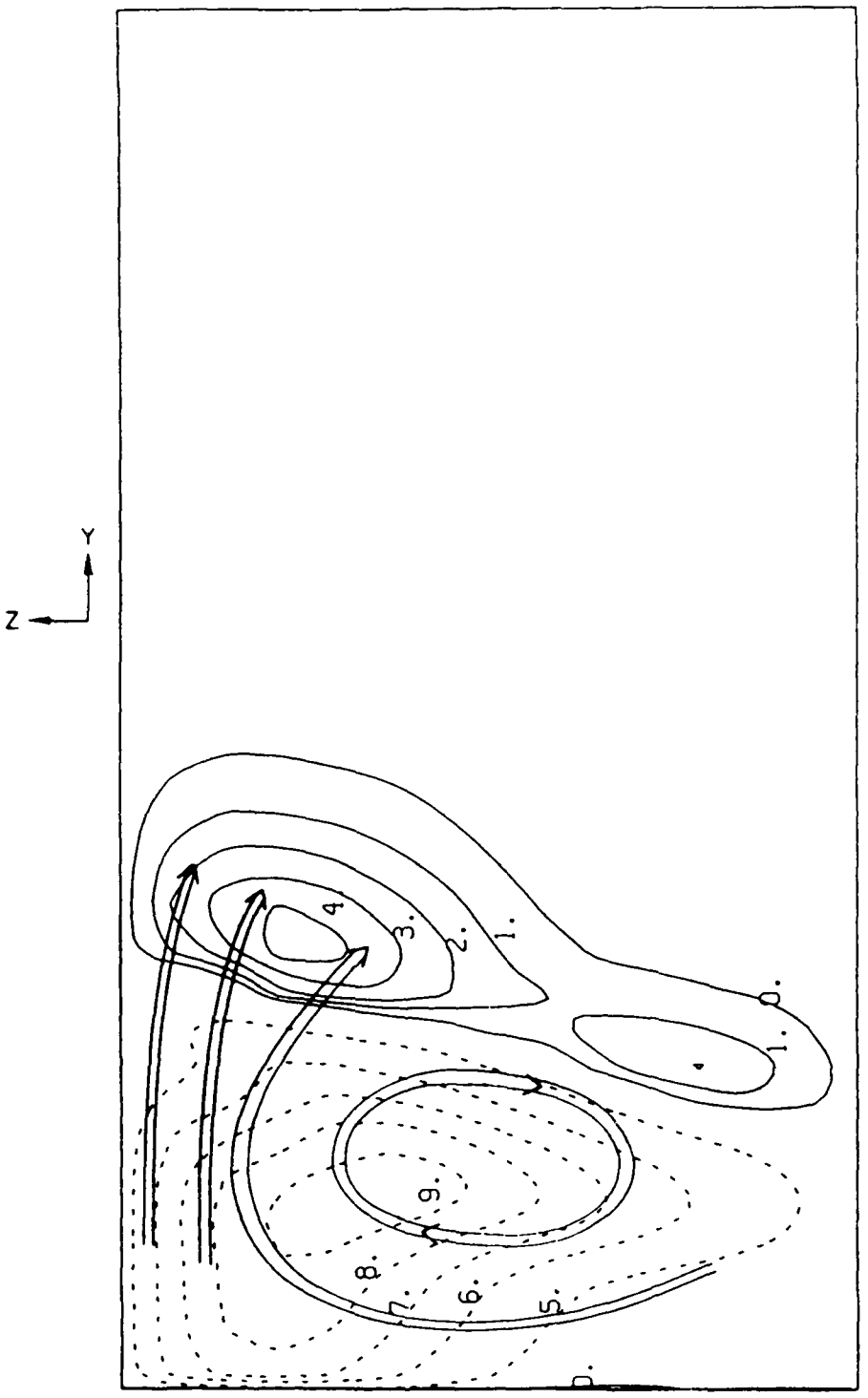

Fig. 17. Production of streamwise vorticity due to straining at t=0.11.
(f_{max}=5.5560, f_{min}=-62.485

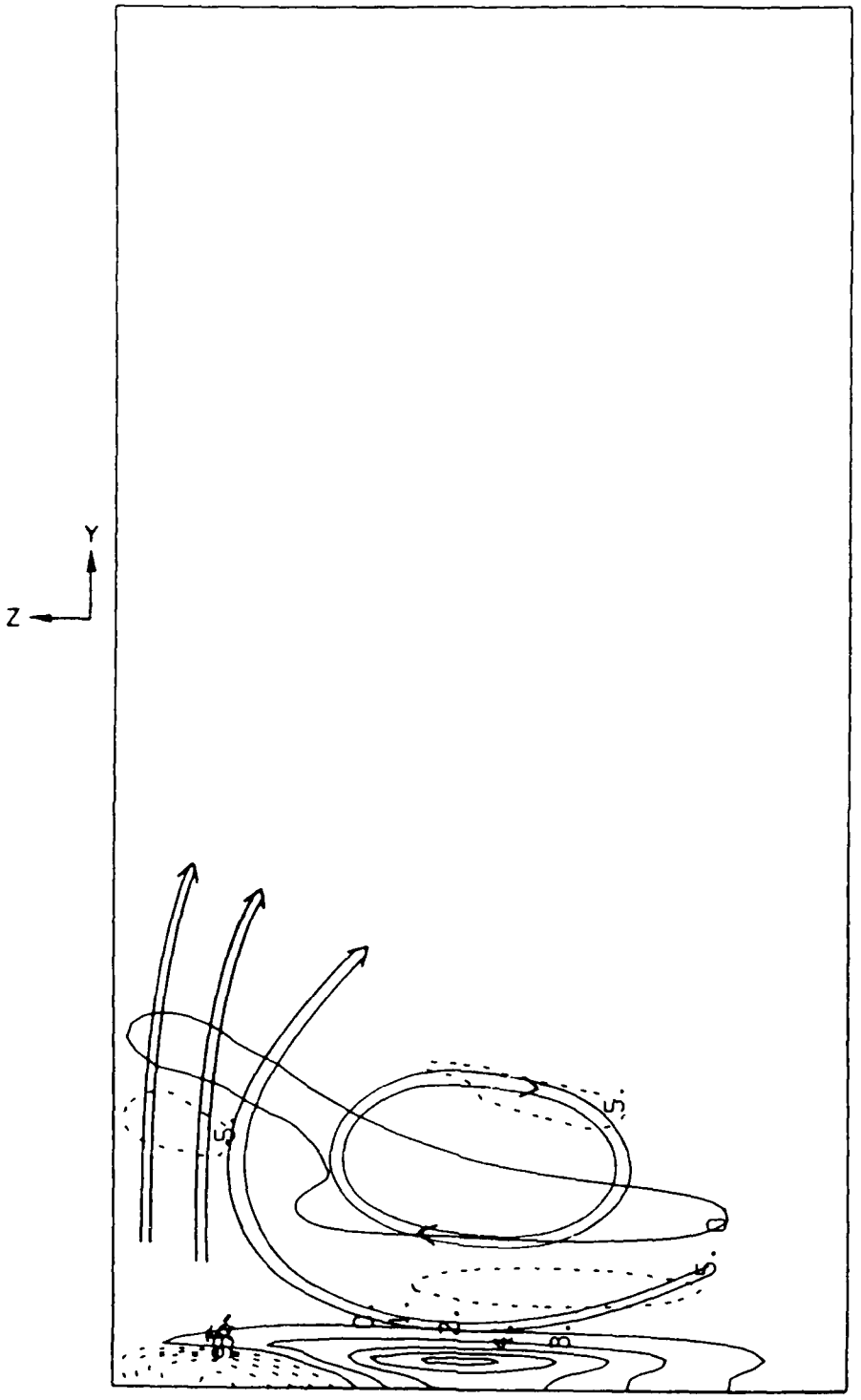

Fig. 18. Transfer of streamwise vorticity due to viscous diffusion at t=0.11.
(f_{max}=50.3037, f_{min}=-38.0548)

Fig. 19. Production of normal vorticity due to straining at t=0.11.
(f_{max}=17.8591, f_{min}=-41.7403)

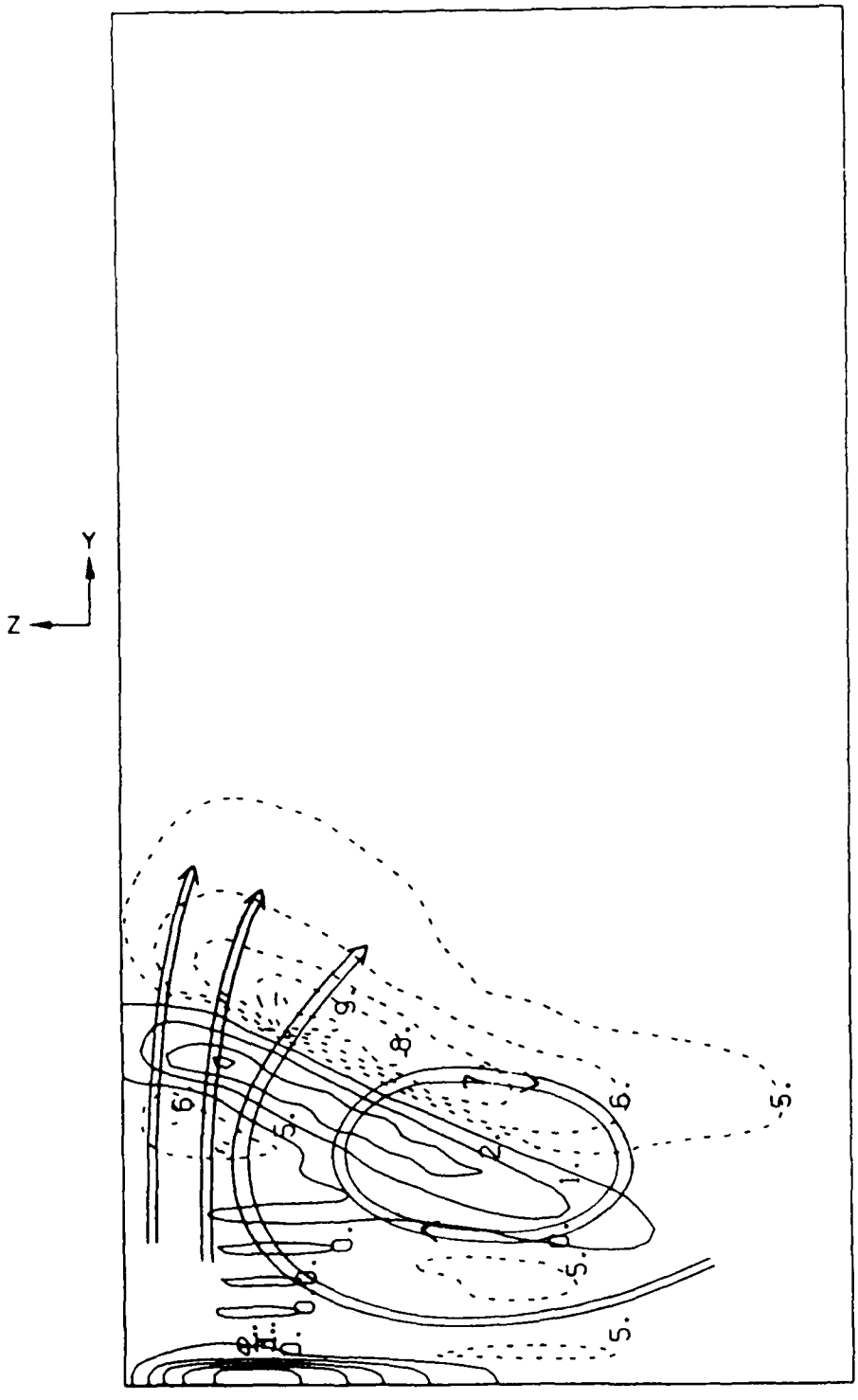

Fig. 20. Transfer of normal vorticity due to viscous diffusion at t=0.11. (f_{max}=21.2264, f_{min}=-6.1281)

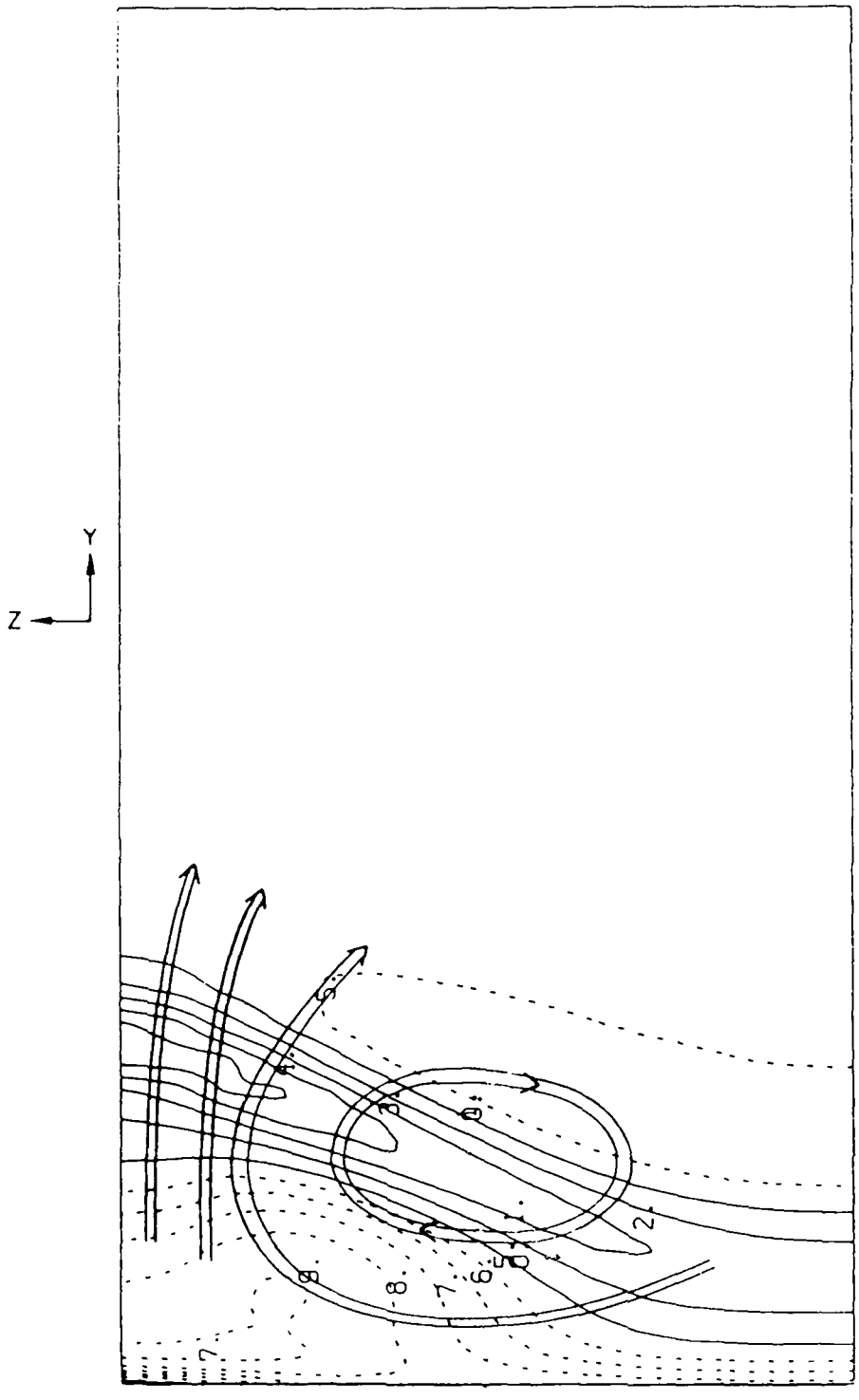

Fig. 21. Variation of dissipation per unit mass from the Blasius flow at t=0.11. (f_{max}=0.0123, f_{min}=-0.0084)

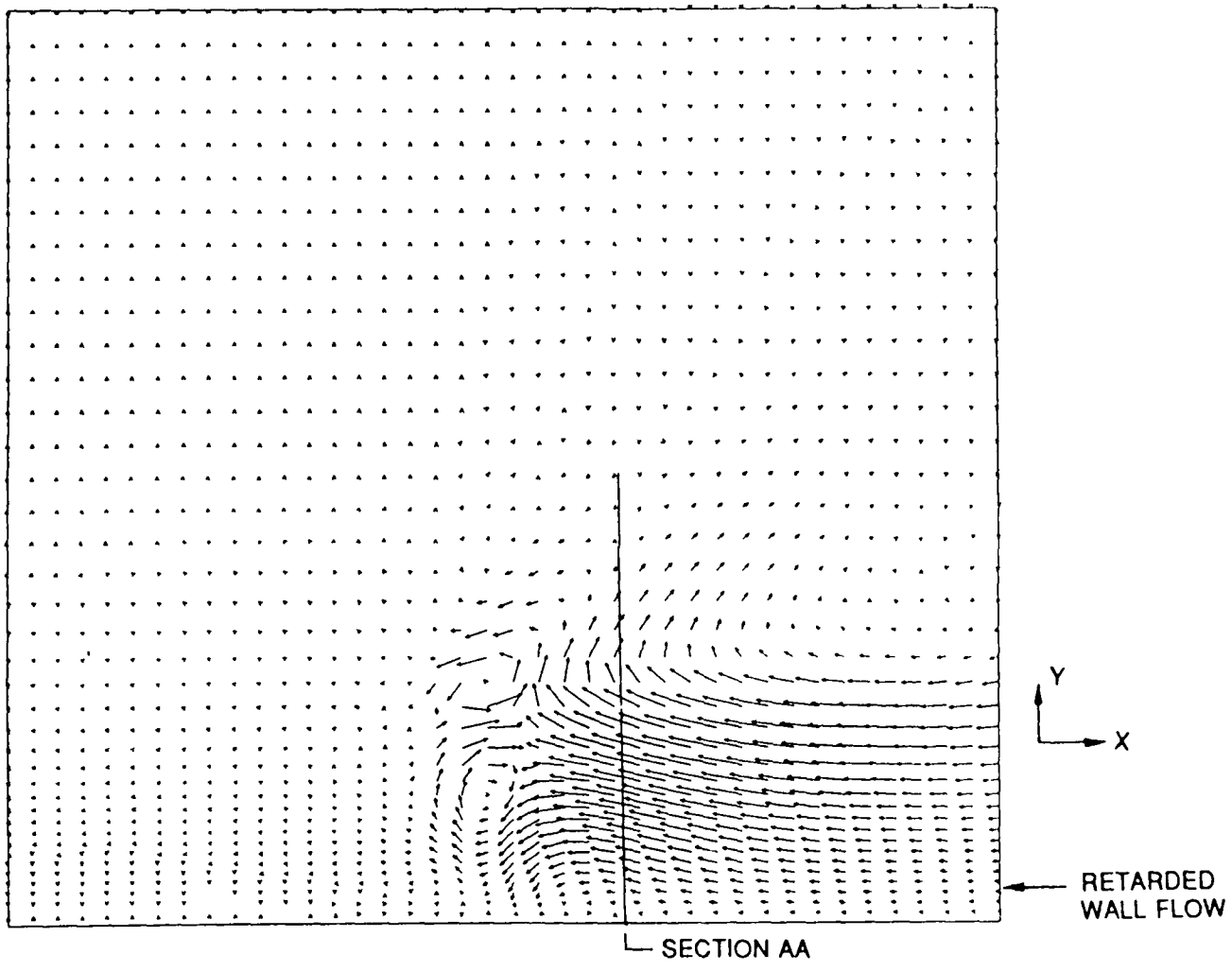

Fig. 22. Variation of projected vector field from Blasius flow.
(center plane, side view, t=0.11)
(q_{max}=0.058)

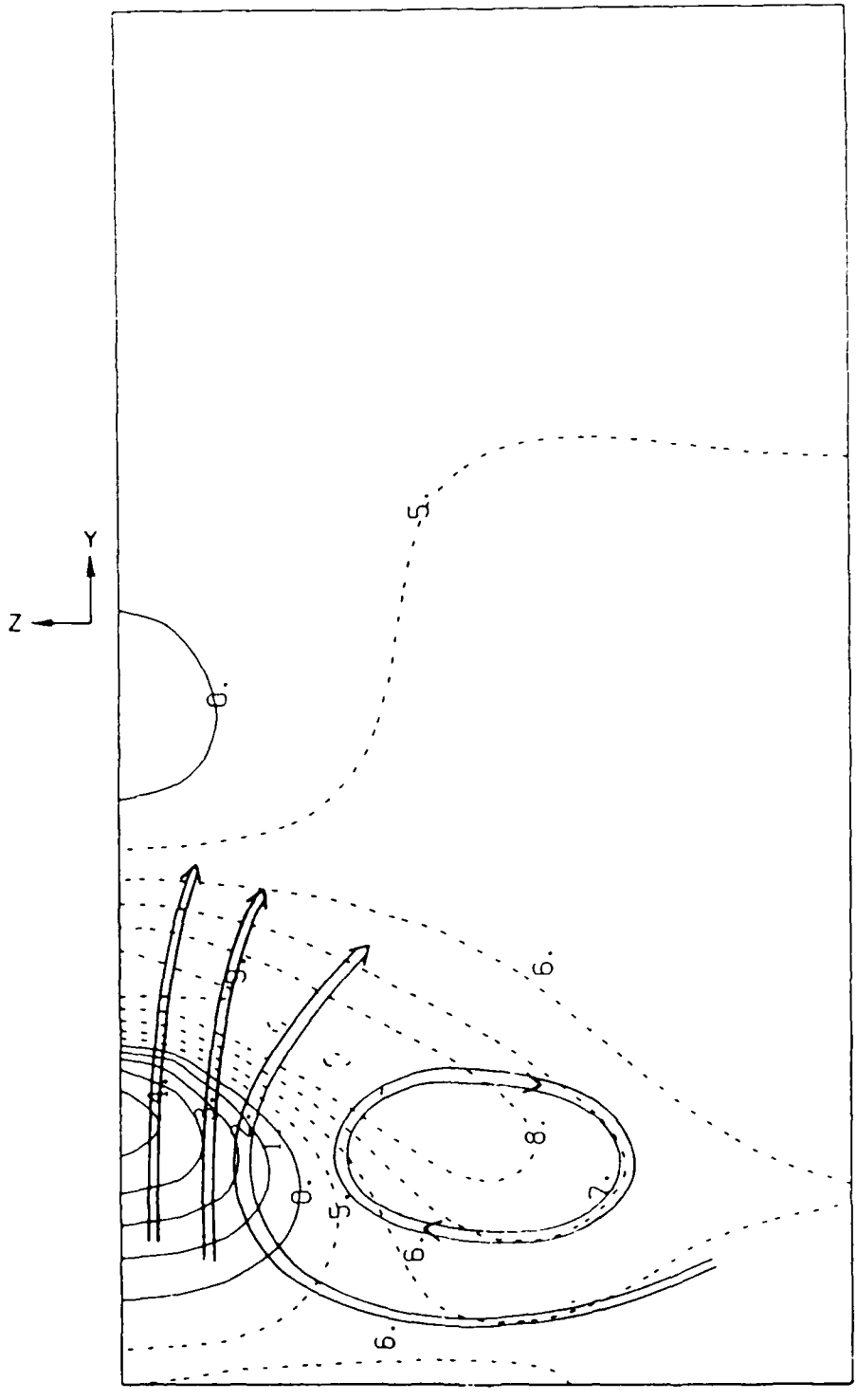

Fig. 23. Static pressure coefficient ($0.5C_p$) at t=0.11.
(f_{max}=0.1045×10^{-1}, f_{min}=-0.1135×10^{-1})

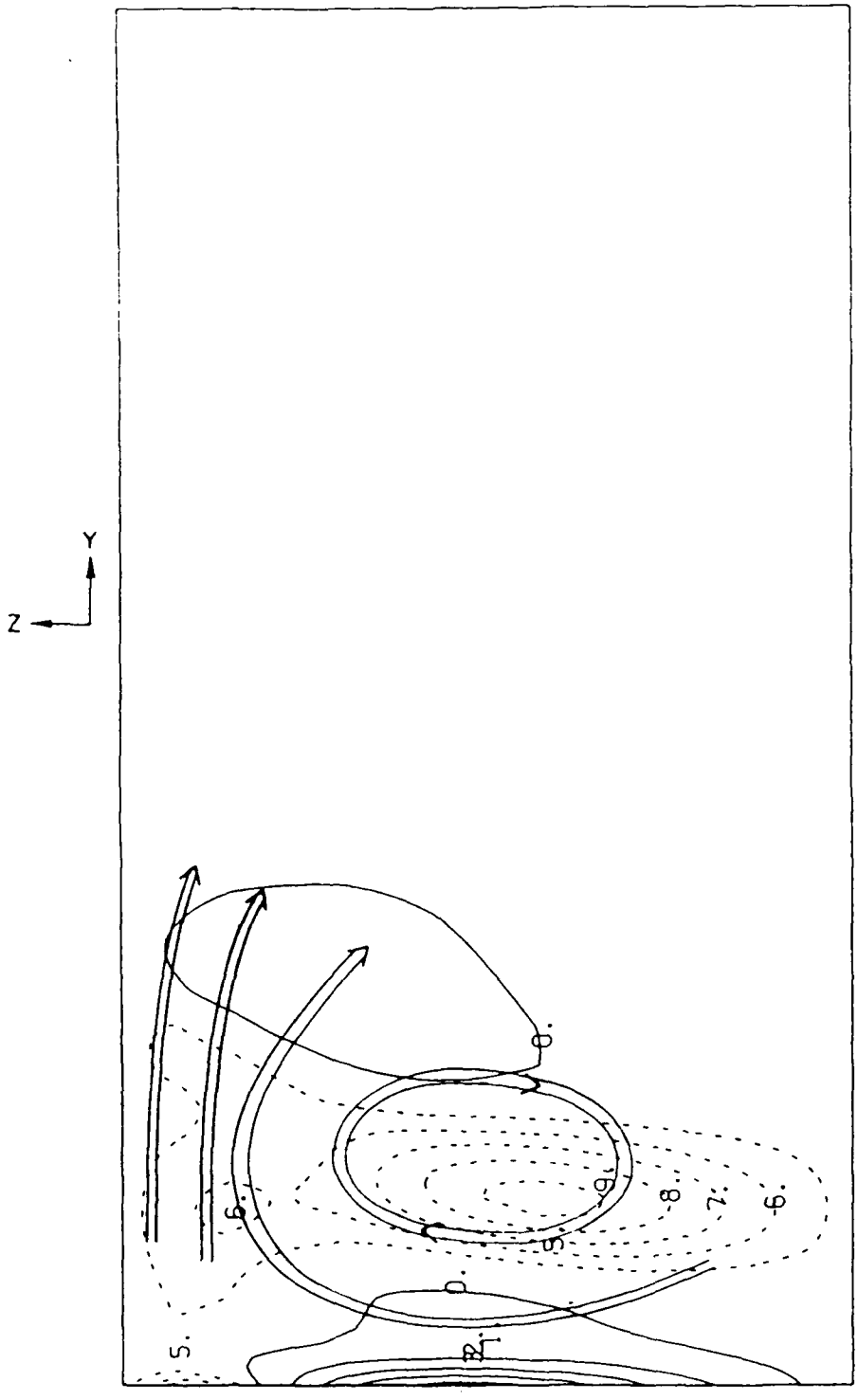

Fig. 24. Distribution of shear stress, S_{yz} at t=0.11.
(f_{max}=0.365x10^{-3}, f_{min}=-0.122x10^{-3})

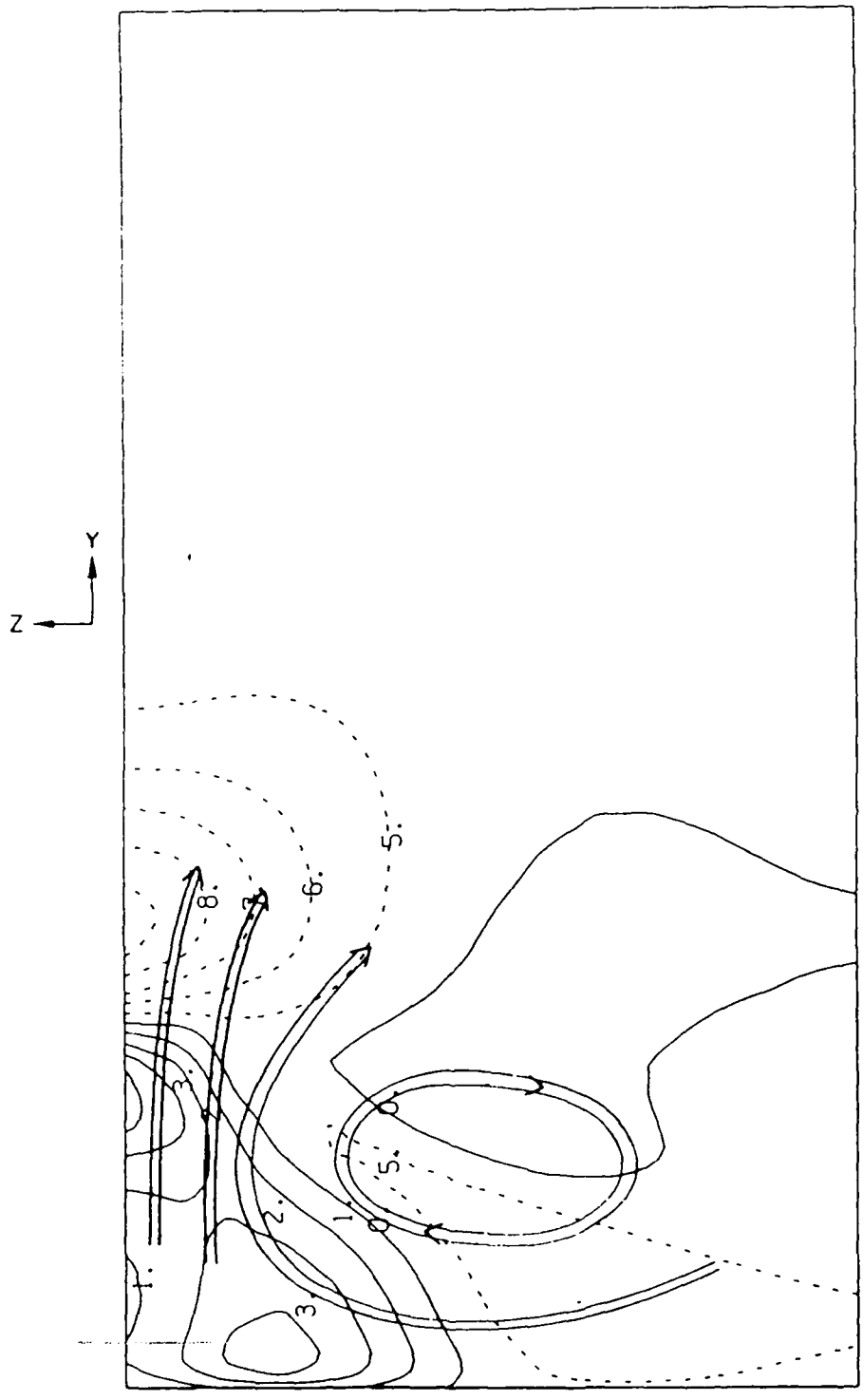

Fig. 25. Distribution of normal stress, S_{yy} at t=0.11.
(f_{max}=0.123x10^{-3}, f_{min}=-0.139x10^{-3})

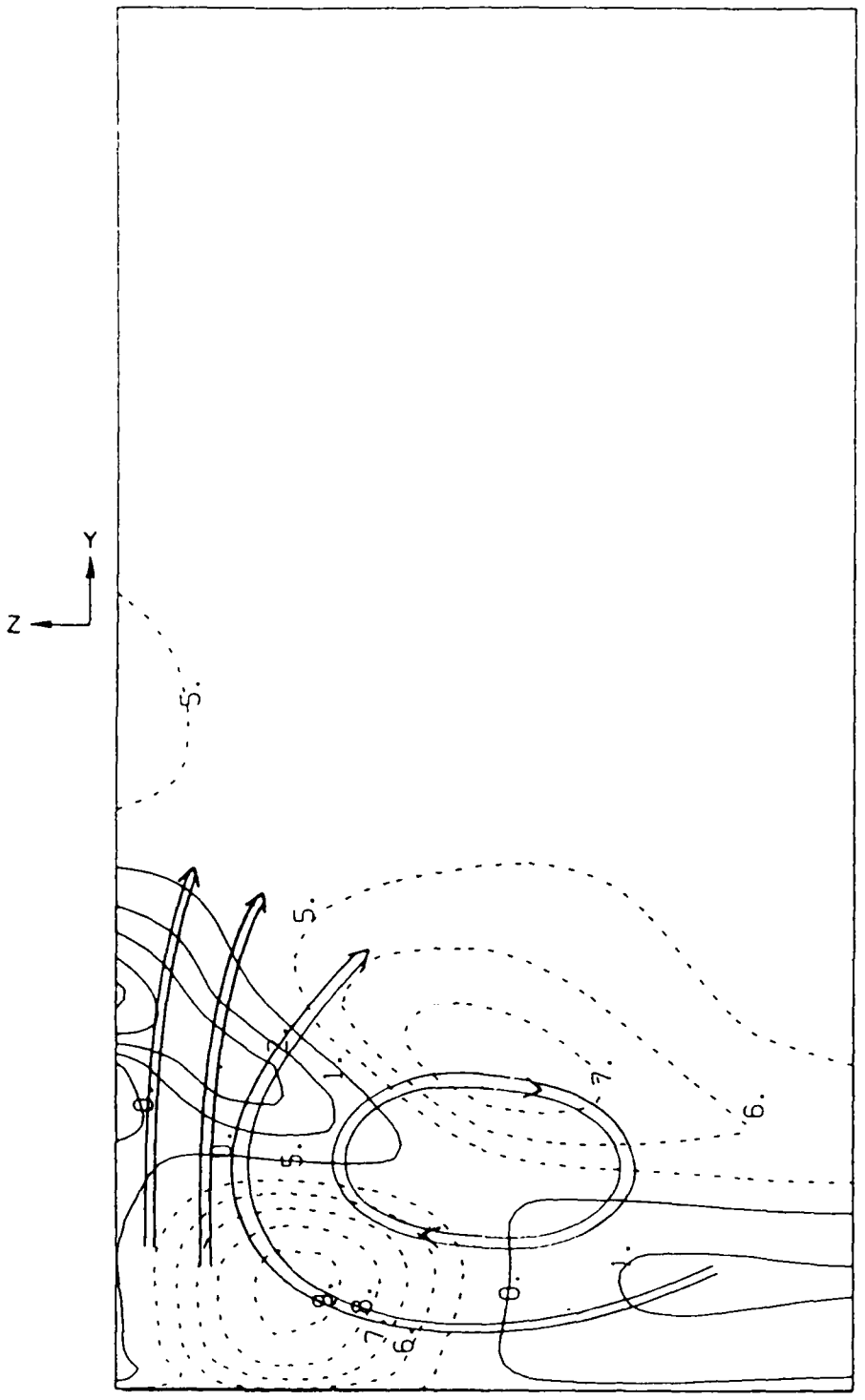

Fig. 26. Distribution of normal stress, S_{zz} at t=0.11.
(f_{max}=0.170x10^{-3}, f_{min}=-0.083x10^{-3})

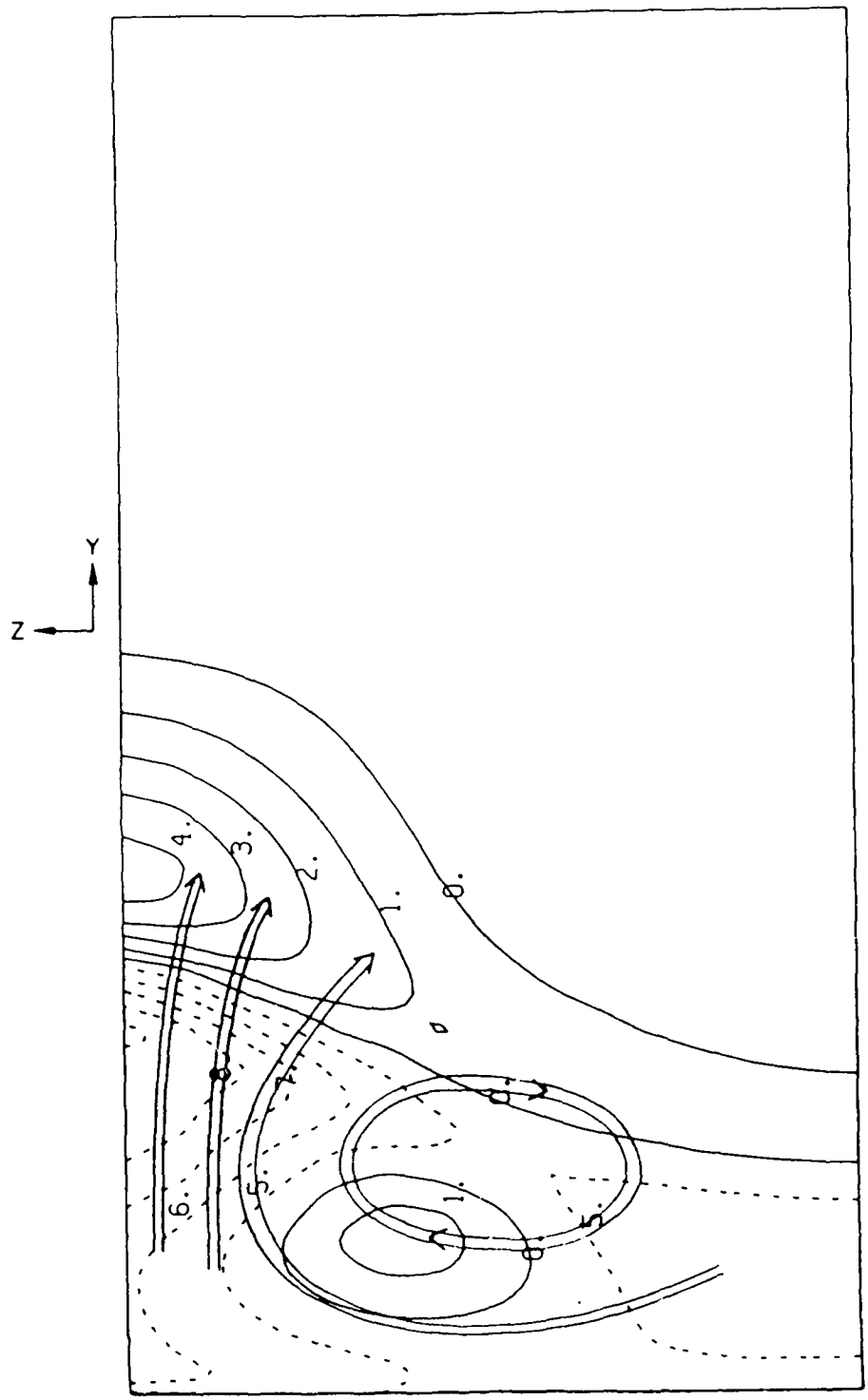

Fig. 27. Distribution of normal stress, S_{xx} at t=0.11.
(f_{max}=0.097x10^{-3}, f_{min}=-0.159x10^{-3})

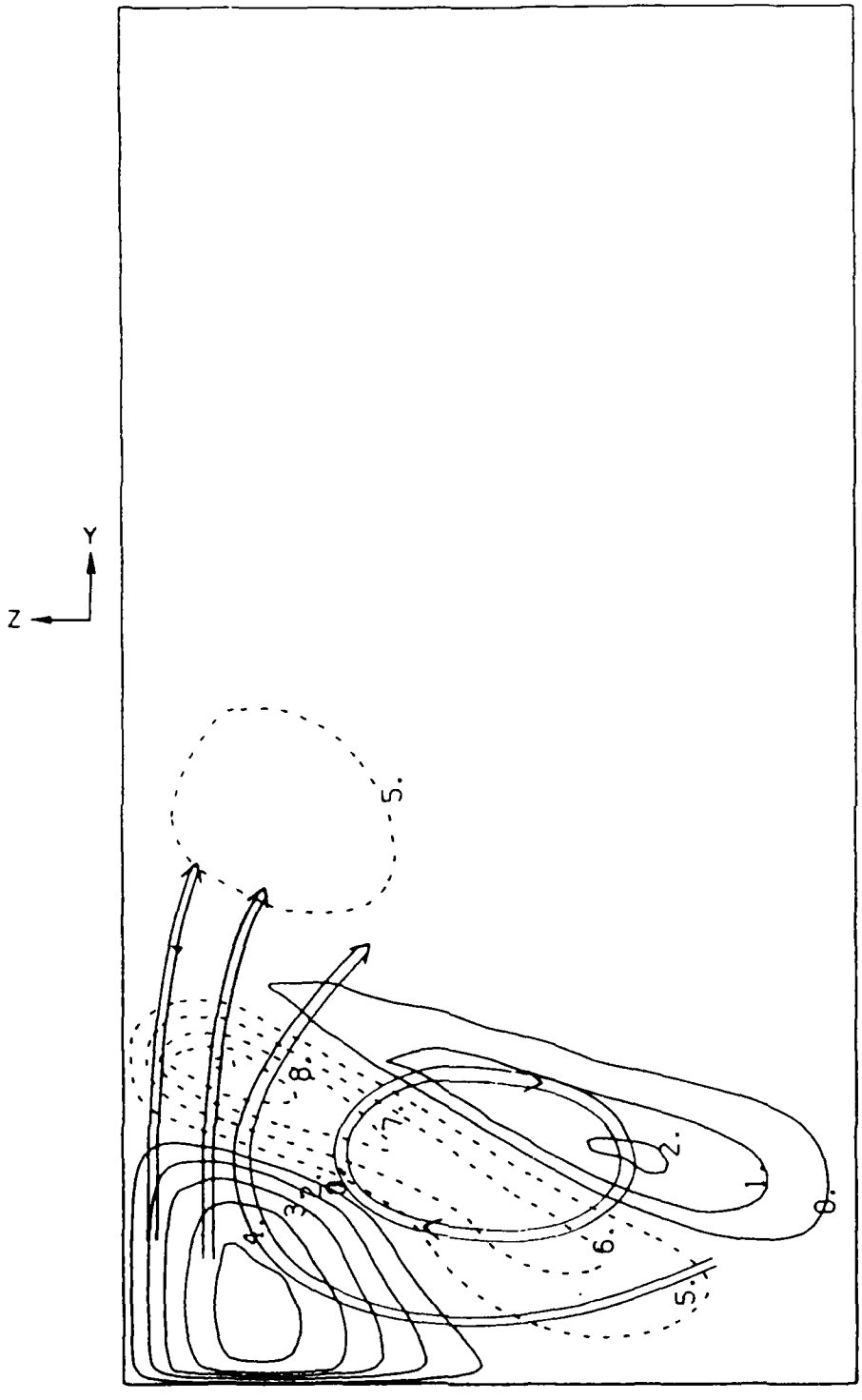

Fig. 28. Distribution of shear stress, S_{xz} at t=0.11.
(f_{max}=0.062x10^{-3}, f_{min}=-0.112x10^{-3})

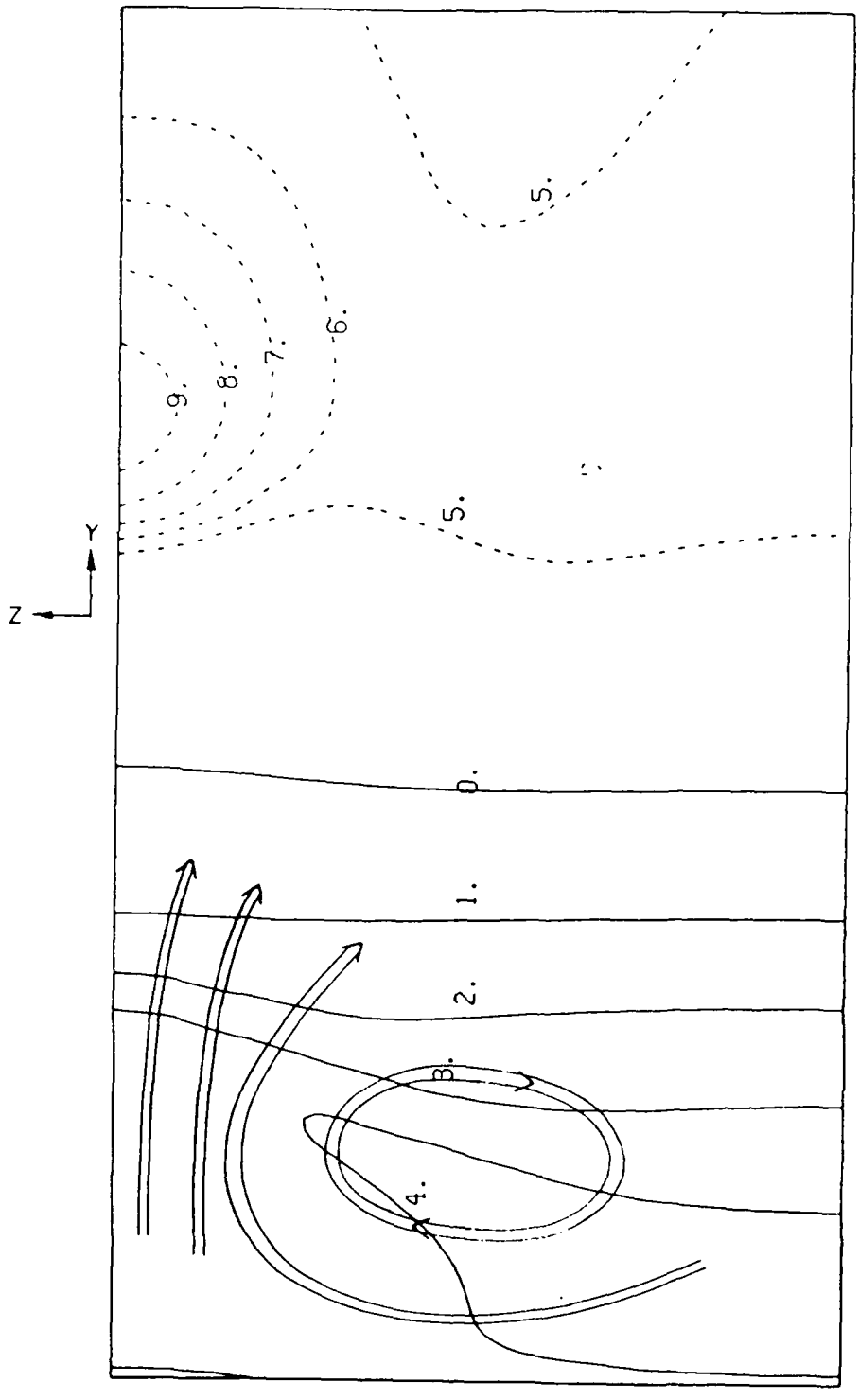

Fig. 29. Distribution of shear stress, S_{xy} at t=0.11.
(f_{max}=1.223x10^{-3}, f_{min}=-0.008x10^{-3})

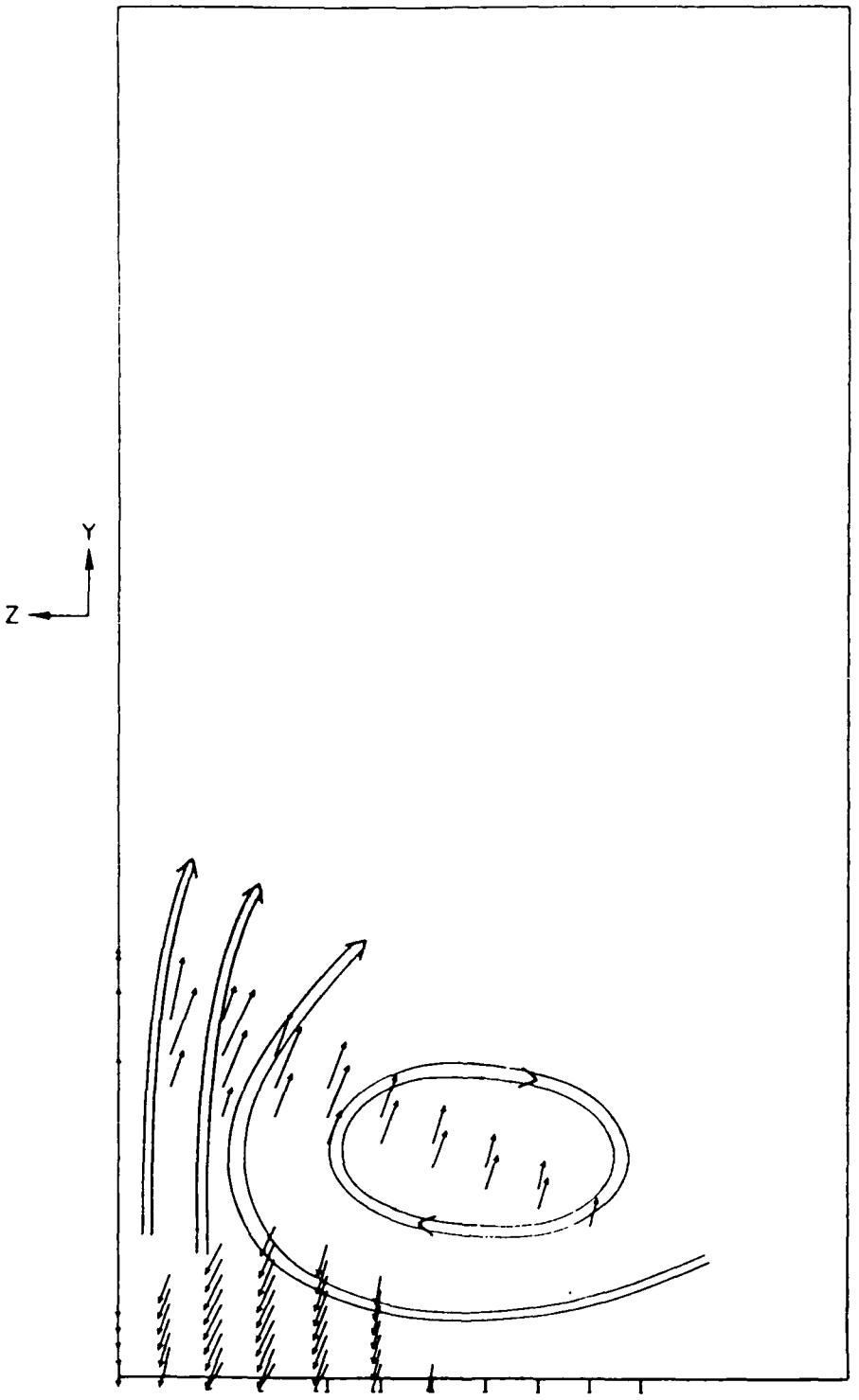

Fig. 30. Variation of shear stress vector from the Blasius flow at t=0.11.

END

DATE

FILMED

8-88

DTIC